Modelling spinal circuitry involved in locomotor pattern generation: insights from deletions during fictive locomotion

Ilya A. Rybak[1], Natalia A. Shevtsova[1,2], Myriam Lafreniere-Roula[3] and David A. McCrea[3]

[1]*Department of Neurobiology and Anatomy, Drexel University College of Medicine, Philadelphia, PA 19129, USA*
[2]*A. B. Kogan Research Institute for Neurocybernetics, Rostov State University, Rostov-on-Don 344090, Russia*
[3]*Spinal Cord Research Centre and Department of Physiology, University of Manitoba, Winnipeg, Manitoba R3E 3J7, Canada*

The mammalian spinal cord contains a locomotor central pattern generator (CPG) that can produce alternating rhythmic activity of flexor and extensor motoneurones in the absence of rhythmic input and proprioceptive feedback. During such fictive locomotor activity in decerebrate cats, spontaneous omissions of activity occur simultaneously in multiple agonist motoneurone pools for a number of cycles. During these 'deletions', antagonist motoneurone pools usually become tonically active but may also continue to be rhythmic. The rhythmic activity that re-emerges following a deletion is often not phase shifted. This suggests that some neuronal mechanism can maintain the locomotor period when motoneurone activity fails. To account for these observations, a simplified computational model of the spinal circuitry has been developed in which the locomotor CPG consists of two levels: a half-centre rhythm generator (RG) and a pattern formation (PF) network, with reciprocal inhibitory interactions between antagonist neural populations at each level. The model represents a network of interacting neural populations with single interneurones and motoneurones described in the Hodgkin-Huxley style. The model reproduces the range of locomotor periods and phase durations observed during real locomotion in adult cats and permits independent control of the level of motoneurone activity and of step cycle timing. By altering the excitability of neural populations within the PF network, the model can reproduce deletions in which motoneurone activity fails but the phase of locomotor oscillations is maintained. The model also suggests criteria for the functional identification of spinal interneurones involved in the mammalian locomotor pattern generation.

(Resubmitted 4 August 2006; accepted after revision 24 September 2006; first published online 28 September 2006)
Corresponding author D. A. McCrea: Spinal Cord Research Centre, University of Manitoba, 730 William Avenue, Winnipeg, Manitoba, R3E3J7 Canada. Email: dave@scrc.umanitoba.ca

Locomotor central pattern generator in the mammalian spinal cord

It is widely accepted that the mammalian spinal cord contains a central pattern generator (CPG) that can produce the basic locomotor rhythm in the absence of rhythmic input from higher brain centres and peripheral sensory feedback (Graham Brown, 1911; Grillner, 1981; Rossignol, 1996; Orlovsky *et al.* 1999). Although the neuronal organization of this CPG remains largely unknown, there appears to be at least one CPG for each hindlimb because the hindlimbs of cats with chronic thoracic spinal lesions can step at independent rates (Forssberg *et al.* 1980). Graham Brown (1914) offered the first conceptual scheme of the mammalian CPG based on a half-centre concept. According to this concept, the locomotor rhythm results from interplay between tonic excitation of two populations of excitatory interneurones (referred to as half-centres) and the reciprocal inhibition between them. Each half-centre excites synergist motoneurones and activates interneurones inhibiting antagonist motoneurones (e.g. Jankowska *et al.* 1967*a*,*b*; Lundberg, 1981). In this organization, a single network controls the rhythm and pattern of motoneurone activity during locomotion.

To overcome some of the inherent limitations of a single CPG network and provide for a variety of motoneurone recruitment patterns, Grillner (1981) suggested that subsets of motoneurone pools are controlled by multiple, coupled, unit burst generators (UBGs) (see also Stein & Smith, 1997). Others have suggested that a bipartite (half-centre) organization can also sculpt the activity of individual motoneurone pools if additional neural circuits operate between the rhythm generator (RG) and

 DOI: 10.1113/jphysiol.2006.118703

motoneurones. Such intermediate neural circuits have been proposed to reproduce the complex pattern of activity in motoneurone pools innervating bifunctional muscles or to provide a separation of the tasks of rhythm generation and motoneurone activation during locomotion (Perret & Cabelguen, 1980; Perret, 1983; Koshland & Smith, 1989; Kriellaars *et al.* 1994; Burke *et al.* 2001).

Insights into CPG organization from experimental studies of fictive locomotion

Continuous electrical stimulation of the midbrain locomotor region (MLR) in the immobilized decerebrate cat produces 'fictive locomotion' consisting of rhythmic alternating activation of flexor and extensor motoneurones similar to that occurring during normal locomotion in the intact animal (see Rossignol, 1996). Two types of experimental studies of fictive locomotion in our laboratory motivated the development of the CPG architecture presented here. The first was an investigation of the effects of stimulation of hindlimb sensory afferents on motoneurone activity and step cycle timing (e.g. Guertin *et al.* 1995; Perreault *et al.* 1995; McCrea, 2001; Stecina *et al.* 2005). These studies revealed that in many cases, afferent stimulation can delay or cause a premature phase switching within the ongoing step cycle without changing the timing of the following step cycles (see the following paper, Rybak *et al.* 2006).

The other experimental findings that motivated the present study came from an investigation of 'deletions' – spontaneous errors in the rhythmic activity of motoneurones occurring during fictive locomotion and scratch (Lafreniere-Roula & McCrea, 2005). Such deletions of rhythmic motoneurone activity have been observed during fictive (e.g. Grillner & Zangger, 1979) and treadmill locomotion in cats (e.g. Duysens, 1977) and extensively described in turtles during the scratch reflex (e.g. Stein & Grossman, 1980; Stein, 2005). Deletions observed during fictive locomotion in cats are characterized by brief periods of inactivity occurring simultaneously in multiple synergist motoneurone populations. During these deletions, the activity of antagonist motoneurone populations usually becomes tonic but may continue to be rhythmic (Lafreniere-Roula & McCrea, 2005). The widespread effect of deletions on the activity of multiple motoneurone pools throughout the limb is strong evidence that they are produced by failures in the operation of some common spinal circuitry, such as the CPG, and not a result of local perturbations affecting the excitability of particular motoneurones.

An analysis of motoneurone activities during and following deletions revealed that some deletions are accompanied by a resetting of the rhythm which can be recognized by a shift in the phase of the re-emerging rhythm relative to the rhythm preceding the deletion (Lafreniere-Roula & McCrea, 2005). Such rhythm resetting or phase shifting after a deletion can be easily explained within the framework of the classical half-centre CPG organization. For example, because of reciprocal inhibition between the half-centres, a spontaneous temporary increase in the excitability of one half-centre would cause an inhibition of the antagonist half-centre, resulting in a deletion of the activity of the corresponding antagonist motoneurone pools. As the duration of the perturbation causing the deletion may be arbitrary, the rhythm following the perturbation should generally be accompanied by a shift of the phase of the post-deletion rhythm relative to the pre-deletion rhythm.

Most spontaneous deletions observed during fictive locomotion are characterized, however, by a maintenance of the phase of locomotor oscillations after the deletion (Lafreniere-Roula & McCrea, 2005). Thus the bursts of motoneurone activity that re-emerge after a deletion often occur at an integer number of the missing locomotor periods. In other words, the post-deletion motoneurone bursts appear at the times which would have been expected if the deletion had not occurred (i.e. the locomotor rhythm is not reset) (Lafreniere-Roula & McCrea, 2005). These observations suggest that the internal structure of the CPG can 'remember' and maintain the locomotor cycle period when motoneurone activity falls silent. Such rhythm and phase maintenance is inconsistent with the classical half-centre CPG organization, in which a single network is responsible for both rhythm generation and motoneurone activation.

The present study explores a novel architecture of the locomotor CPG that incorporates features of both the half-centre and the UBG organizations. In order to explain the above experimental findings, we suggest that the locomotor CPG has a two-level architecture containing a half-centre RG, performing a 'clock' function, and an intermediate pattern formation (PF) network that distributes and coordinates the activities of multiple motoneurone populations (see Fig. 1). The RG defines the locomotor rhythm and durations of flexor and extensor phases. It also controls the activity of the PF network interposed between the RG and motoneurones. The PF network contains multiple interneurone populations each of which projects to multiple synergist motoneurone populations and reciprocally inhibits other populations within the PF network. Depending on the input from the RG network and the interactions within the PF network, each PF population is active during a particular phase(s) of the step cycle and produces a phase-specific synchronized activation of the corresponding group of synergist motoneurone pools (see Fig. 1).

The hypothesized two-level organization of the CPG allows a separate control of the locomotor rhythm (at the RG level) and the pattern of motoneurone activations (at the PF level). Consequently, sensory

signals or a spontaneously occurring perturbation may affect CPG operation at the RG level, altering the locomotor rhythm (e.g. producing a phase shift or rhythm resetting) or act at the PF level, altering the pattern of motoneurone activation without resetting the rythm or shifting the phase (see Fig. 1). In the present report we describe a computational model representing a reduced version of the above conceptual model and compare the results of modelling with the experimental study of deletions observed during MLR-evoked fictive locomotion in decerebrate cats. Modelling the effects of afferent stimulation on the locomotor rhythm and pattern is presented in the following paper (Rybak *et al.* 2006). Some results have been presented in abstract form (Rybak *et al.* 2004*a*; Rybak & McCrea, 2005).

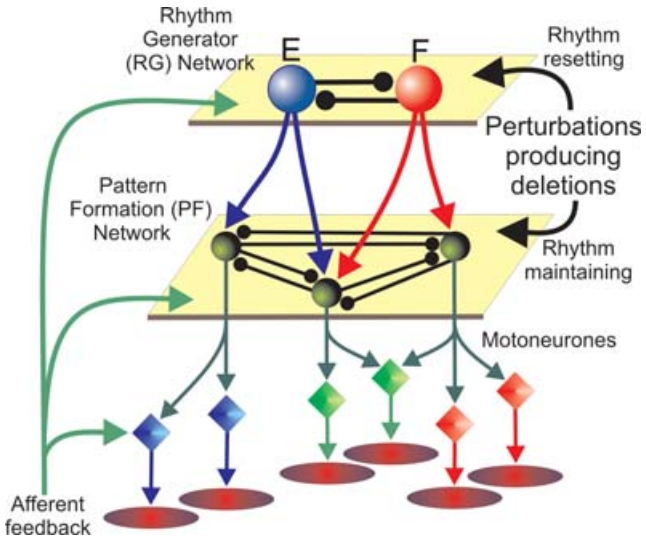

Figure 1. Schematic illustration of the two-level central pattern generator (CPG) concept
The locomotor CPG consists of a half-centre rhythm generator (RG) and a pattern formation (PF) network. The RG defines the locomotor rhythm and the durations of flexor and extensor phases and controls the activity of the PF network. The PF network contains interneurone populations (green spheres), each of which provides excitation to multiple synergist motoneurone pools (diamonds) and is connected with other PF populations via a network of inhibitory connections. Activation of a particular PF population activates the corresponding muscle synergy. The PF network mediates rhythmic input from the RG to motoneurones and distributes it among the motoneurone pools. Depending on the input from the RG and the interactions within the PF network, each PF population is active within particular phase(s) of the step cycle and produces a phase-specific, synchronized activation of the corresponding group of synergist motoneurone pools. Afferent feedback and spontaneous perturbations may affect the CPG either at the level of the RG, producing alterations (e.g. phase shifting or resetting) of the locomotor rhythm, or at the level of PF, altering the level of motoneurone activation and/or the timing of phase transitions without shifting the phase of (or resetting) the locomotor rhythm generated by the RG. See details in the text.

Methods

Models of single motoneurones and interneurones

All neurones were modelled in the Hodgkin-Huxley style. Interneurones were simulated as single-compartment models. Motoneurones had two compartments: soma and dendrite. In this study, we accepted and used the two-compartment motoneurone model described by Booth *et al.* (1997). In accordance with this model, the following ionic currents (with the corresponding channel conductances) have been considered: fast sodium (I_{Na} with maximal conductance $\bar{g}_{Na}$); delayed-rectifier potassium (I_K with maximal conductance $\bar{g}_K$); calcium-N (I_{CaN} with maximal conductance $\bar{g}_{CaN}$); calcium-L (I_{CaL} with maximal conductance $\bar{g}_{CaL}$), calcium-dependent potassium ($I_{K,Ca}$ with maximal conductance $\bar{g}_{K,Ca}$), and leakage (I_L with constant conductance g_L) currents. In addition, based on evidence for the presence of the persistent (slowly inactivating) sodium current (I_{NaP}) in spinal cord interneurones and motoneurones (Lee & Heckman, 2001; Darbon *et al.* 2004; Streit *et al.* 2005), this current has been also included in our neurone models (with maximal conductance $\bar{g}_{NaP}$). The above ionic currents are described as follows:

$$\begin{aligned} I_{Na} &= \bar{g}_{Na} \times m_{Na}^3 \times h_{Na} \times (V - E_{Na});\\ I_{NaP} &= \bar{g}_{NaP} \times m_{NaP} \times h_{NaP} \times (V - E_{Na});\\ I_K &= \bar{g}_K \times m_K^4 \times (V - E_K);\\ I_{CaN} &= \bar{g}_{CaN} \times m_{CaN}^2 \times h_{CaN} \times (V - E_{Ca});\\ I_{CaL} &= \bar{g}_{CaL} \times m_{CaL} \times (V - E_{Ca});\\ I_{K,Ca} &= \bar{g}_{K,Ca} \times m_{K,Ca} \times (V - E_K);\\ I_L &= g_L \times (V - E_L), \end{aligned} \tag{1}$$

where V is the membrane potential of the corresponding neurone compartment (i.e. soma ($V_{(S)}$) or dendrite ($V_{(D)}$)) in two-compartment models, or the neurone membrane potential V in one-compartment models; E_{Na}, E_K, E_{Ca} and E_L are the reversal potentials for sodium, potassium, calcium and leakage currents, respectively; variables m and h with indices indicating ionic currents represent, respectively, the activation and inactivation variables of the corresponding ionic channels.

The dendrite–soma coupling currents (with conductance g_C) for soma ($I_{C(S)}$) and dendrite ($I_{C(D)}$) are described following the Booth *et al.* (1997) model:

$$\begin{aligned} I_{C(S)} &= \frac{g_C}{p} \times (V_{(S)} - V_{(D)});\\ I_{C(D)} &= \frac{g_C}{1-p} \times (V_{(D)} - V_{(S)}), \end{aligned} \tag{2}$$

where p is the parameter defining the ratio of somatic surface area to total surface area.

Synaptic excitatory (I_{SynE} with conductance g_{SynE} and reversal potential E_{SynE}) and inhibitory (I_{SynI} with conductance g_{SynI} and reversal potential E_{SynI}) currents have also been incorporated into our models:

$$\begin{aligned} I_{\mathrm{SynE}} &= g_{\mathrm{SynE}} \times (V - E_{\mathrm{SynE}}); \\ I_{\mathrm{SynI}} &= g_{\mathrm{SynI}} \times (V - E_{\mathrm{SynI}}). \end{aligned} \tag{3}$$

The kinetics of intracellular Ca^{2+} concentration (Ca, described separately for each compartment) is modelled according to the following equation (Booth *et al.* 1997):

$$\frac{\mathrm{d}}{\mathrm{d}t}Ca = f \times (-\alpha \times I_{\mathrm{Ca}} - k_{\mathrm{Ca}} \times Ca), \tag{4}$$

where f defines the percentage of free to total Ca^{2+}, α converts the total Ca^{2+} current, I_{Ca}, to Ca^{2+} concentration and k_{Ca} represents the Ca^{2+} removal rate.

In accordance with the two-compartment motoneurone model of Booth *et al.* (1997) but with the inclusion of I_{NaP} to the motoneurone dendrite, the membrane potentials of the motoneurone soma ($V_{(\mathrm{S})}$) and dendrite ($V_{(\mathrm{D})}$) are described by the following differential equations:

$$\begin{aligned} C \times \frac{\mathrm{d}V_{(\mathrm{S})}}{\mathrm{d}t} &= -I_{\mathrm{Na(S)}} - I_{\mathrm{K(S)}} - I_{\mathrm{CaN(S)}} \\ &\quad -I_{\mathrm{K,Ca(S)}} - I_{\mathrm{L(S)}} - I_{\mathrm{C(S)}}; \\ C \times \frac{\mathrm{d}V_{(\mathrm{D})}}{\mathrm{d}t} &= -I_{\mathrm{NaP(D)}} - I_{\mathrm{CaN(D)}} - I_{\mathrm{CaL(D)}} - I_{\mathrm{K,Ca(D)}} \\ &\quad -I_{\mathrm{L(D)}} - I_{\mathrm{C(D)}} - I_{\mathrm{SynE}} - I_{\mathrm{SynI}}, \end{aligned} \tag{5}$$

where C is the membrane capacitance and t is time.

For simplicity and because of the lack of specific data, all interneurones (single-compartment models) except RG and PF neurons contain only a minimal set of ionic currents:

$$C \times \frac{\mathrm{d}V}{\mathrm{d}t} = -I_{\mathrm{Na}} - I_{\mathrm{K}} - I_{\mathrm{L}} - I_{\mathrm{SynE}} - I_{\mathrm{SynI}}. \tag{6}$$

The excitatory neurons of the CPG comprising the RG and PF populations have the persistent (slowly inactivating) sodium current, I_{NaP}, which has been suggested to play an important role in the intrinsic rhythmogenesis in spinal interneurones (Darbon *et al.* 2004; Streit *et al.* 2005). The membrane potential of these interneurones is described as follows:

$$C \times \frac{\mathrm{d}V}{\mathrm{d}t} = -I_{\mathrm{Na}} - I_{\mathrm{NaP}} - I_{\mathrm{K}} - I_{\mathrm{L}} - I_{\mathrm{SynE}} - I_{\mathrm{SynI}}. \tag{7}$$

Activation m and inactivation h of voltage-dependent ionic channels (e.g. Na^+, $Na_P{}^+$, K^+, $Ca_N{}^{2+}$, $Ca_L{}^{2+}$) are described by the following differential equations:

$$\begin{aligned} \tau_{mi}(V) \times \frac{\mathrm{d}}{\mathrm{d}t}m_i &= m_{\infty i}(V) - m_i; \\ \tau_{hi}(V) \times \frac{\mathrm{d}}{\mathrm{d}t}h_i &= h_{\infty i}(V) - h_i, \end{aligned} \tag{8}$$

where i identifies the name of the channel, $m_{\infty i}(V)$ and $h_{\infty i}(V)$ define the voltage-dependent steady-state activation and inactivation, respectively, and $\tau_{mi}(V)$ and $\tau_{hi}(V)$ define the corresponding time constants (see Table 1 in Appendix). Activation of the sodium channels is considered to be instantaneous ($\tau_{m\mathrm{Na}} = \tau_{m\mathrm{NaP}} = 0$, see Booth *et al.* 1997; Butera *et al.* 1999*a*,*b*).

Activation of the Ca^{2+}-dependent potassium channels is also considered instantaneous and described as follows (Booth *et al.* 1997):

$$m_{\mathrm{K,Ca}} = \frac{Ca}{Ca + K_{\mathrm{d}}}, \tag{9}$$

where Ca is the Ca^{2+} concentration within the corresponding compartment or neurone, and K_{d} defines the half-saturation level of this conductance.

The excitatory (g_{SynE}) and inhibitory synaptic (g_{SynI}) conductances are equal to zero at rest and may be activated (opened) by the excitatory or inhibitory inputs, respectively:

$$\begin{aligned} g_{\mathrm{SynE}i}(t) &= \bar{g}_{\mathrm{E}} \times \sum_j \sum_{<t} S\{w_{ji}\} \times \exp(-(t - t_{kj})/\tau_{\mathrm{SynE}}) \\ &\quad + \bar{g}_{\mathrm{Ed}} \times \sum_m S\{w_{\mathrm{d}mi}\} \times d_{mi}; \\ g_{SynIi}(t) &= \bar{g}_{\mathrm{I}} \times \sum_j \sum_{<t} S\{-w_{ji}\} \times \exp(-(t - t_{kj})/\tau_{\mathrm{SynI}}) \\ &\quad + \bar{g}_{\mathrm{Id}} \times \sum_m S\{-w_{\mathrm{d}mi}\} \times d_{mi}, \end{aligned} \tag{10}$$

where the function $S\{x\} = x$, if $x \geq 0$, and 0 if $x < 0$. The excitatory and inhibitory synaptic conductances in equation (10) ($\mathrm{g_{Sy}E}_i(\mathrm{t})$ and $\mathrm{g_{Syn}I}_i(\mathrm{t})$, respectively) have two terms. The first term describes the integrated effect of inputs from other neurones in the network. The second term describes the integrated effect of inputs from external drive or afferent stimulation d_{mi} (e.g. MLR drive or sensory input from peripheral afferents; see also Rybak *et al.* 1997, 2003). Each spike arriving to neurone i from neurone j at time t_{kj} increases the excitatory synaptic conductance by $\bar{g}_{\mathrm{E}} \times w_{ji}$ if the synaptic weight $w_{ji} > 0$, or increases the inhibitory synaptic conductance by $-\bar{g}_{\mathrm{I}} \times w_{ji}$ if the synaptic weight $w_{ji} < 0$. $\bar{g}_{\mathrm{E}}$ and $\bar{g}_{\mathrm{I}}$ are the parameters defining an increase in the excitatory or inhibitory synaptic conductance, respectively, produced by one arriving spike at $|w_{ji}| = 1$. τ_{SynE} and τ_{SynE} are the decay time constants for the excitatory and inhibitory conductances, respectively. In the second terms of eqn (10), $\bar{g}_{\mathrm{Ed}}$ and $\bar{g}_{\mathrm{Id}}$ are the parameters defining the increase in the excitatory or

inhibitory synaptic conductance, respectively, produced by external input drive $d_{mi} = 1$ with a synaptic weight of $|w_{dmi}| = 1$.

The values of maximal channel conductances and other fixed parameters of neurone models are specified in the Appendix.

Modelling neural populations

In the present model, each functional type of neurone is represented by a population of 20 neurones. Connections between the populations were established such that if population *A* was assigned to receive an excitatory or inhibitory input from population *B* or external drive *D*, then each neurone in population *A* received the corresponding excitatory or inhibitory synaptic input from each neurone in population *B* or from drive *D*, respectively. The heterogeneity of neurones within each population was set by a random distribution of E_L (see mean values ± S.D. in Appendix) and initial conditions for values of membrane potential, calcium concentrations and channel conductances. In all simulations, initial conditions were chosen randomly from a uniform distribution for each variable, and a settling period of 20 s was allowed in each simulation before data were collected. Each simulation was repeated 20–30 times, and demonstrated qualitatively similar behaviour for particular values of E_L and initial conditions taken within the standard deviations.

Computer simulations

All simulations were performed using a simulation package NSM 2.0 (for Windows XP) developed at Drexel University by I. A. Rybak, S. N. Markin and N. A. Shevtsova. Differential equations were solved using the exponential Euler integration method (MacGregor, 1987) with a step of 0.1 ms (further details in Rybak *et al.* 2003).

Recordings from fictive locomotion preparations

This investigation sought to simulate the activity of motoneurones observed during fictive locomotion in decerebrate cats previously described by Lafreniere-Roula & McCrea (2005). No new animal data on motoneurone activity during fictive locomotion were collected. Instead comparisons of simulations from the present model were made with records of electroneurogram (ENG) activity and intracellular recordings from hindlimb motoneurones during fictive locomotion obtained previously (e.g. Lafreniere-Roula & McCrea, 2005). Briefly, those recordings were obtained from precollicular–postmammillary decerebrate cats in which all cortex and rostral brainstem regions were removed before discontinuing the anaesthetic. Surgical and experimental protocols were in compliance with the guidelines set out by the Canadian Council on Animal Care and the University of Manitoba. Fictive locomotion was evoked by electrical stimulation of the midbrain locomoter region (MLR) following neuromuscular blockade. ENG records were rectified and integrated before digitization at 500 Hz and intracellular recordings from lumbar motoneurones were made using sharp glass microelectrodes (for further details, see Lafreniere-Roula & McCrea, 2005). The records in Figs. 9*A*, 10*A*, and 11*A* are taken from Lafreniere-Roula & McCrea (2005) and are used by permission from the American Physiological Society.

Results

Modelling spinal circuits with a two-level locomotor CPG

Because the internal organization of the mammalian CPG remains unknown, our primary goal was to create a model that could demonstrate an important subset of the characteristics of activity seen during fictive locomotion in decerebrate cats. The specific features of locomotion that the model should be able to reproduce were the following. (1) Tonic drive (e.g. constant MLR stimulation) to the CPG should evoke rhythmic activity with two alternating phases ('flexion' and 'extension') coupled without intervening quiescent periods. (2) The model should be able to generate locomotor step cycle periods (T) in the range of 0.4–1.5 s and ratios of flexor (T_F) or extensor (T_E) duration to the period (T_F/T and T_E/T) in the range of 0.25–0.75, observed during fictive locomotion (e.g. Yakovenko *et al.* 2005). (3) Locomotor speed should increase (i.e. the period decrease) with increasing MLR drive (Sirota & Shik, 1973). (4) In the absence of MLR drive, an increase in excitability of CPG neurons should produce a slow locomotor-like activity ($T = 2$–5 s) similar to that evoked by intravenous administration of monoamine precursors in cats *in vivo* (e.g. Jankowska *et al.* 1967*a*,*b*), or by 5-HT in the neonatal rodent isolated spinal cord (e.g. Cowley & Schmidt, 1995; Whelan, 2003). (5) A blockade of synaptic inhibition should trigger synchronized oscillations of flexors and extensors (e.g. Noga *et al.* 1993; Cowley & Schmidt, 1995; Beato & Nistri, 1999).

A consideration of the above features led us to the suggestion that the RG half-centres contain populations of neurons with intrinsic rhythmogenic properties interconnected via mutual excitatory connections within and between the half-centres and that the generation of the locomotor rhythm involves both intrinsic rhythmogenic mechanisms, allowing each half-centre to generate rhythmic activity on its own under certain conditions, and reciprocal inhibitory interactions between the half-centres. While the intrinsic mechanisms defining rhythmogenic properties of CPG neurons remain unknown, there is indirect evidence for the role of

persistent (or slowly inactivating) sodium current, I_{NaP}, in rhythmogenesis. This current is found in spinal cord motoneurones and interneurones (e.g. Lee & Heckman, 2001; Darbon *et al.* 2004; Streit *et al.* 2005) and its blockade by riluzole abolishes intrinsic cellular oscillations and rhythm generation in the networks of cultured rat spinal cord neurons (Darbon *et al.* 2004; Streit *et al.* 2005). Slowly inactivating I_{NaP} has also been found to play a major role in the respiratory rhythm generation in the pre-Bötzinger complex *in vitro* (Butera *et al.* 1999*a,b*) and, under certain conditions, *in vivo* (Rybak *et al.* 2004*b*). Based on this indirect evidence, we incorporated I_{NaP} into the neurons comprising the CPG excitatory populations to provide them with intrinsic rhythmogenic properties similar to those described in the models of the respiratory CPG by Butera *et al.* (1999*b*) and Rybak *et al.* (2003).

The ability of neurones with NaP channels to generate endogenous oscillations is defined by the ratio of the maximal conductance of NaP channels to the maximum conductance of potassium leak (Del Negro *et al.* 2002) and voltage-gated potassium (Rybak *et al.* 2003) channels. If maximal conductances of leak and potassium channels are fixed, then in order for a neurone to generate bursting activity, the maximal conductance of NaP channels should exceed some critical value. In our model, the average value for the maximal conductance for NaP channels in PF neurones was set less than that in RG neurones ($0.1\,mS\,cm^{-2}$ *versus* $0.25\,mS\,cm^{-2}$, see Appendix) and specifically below the level allowing the expression of NaP-dependent rhythmogenic properties under normal conditions. Therefore under normal conditions in our model, the PF network cannot generate its own oscillations, but operates in a forced mode receiving oscillatory inputs from the RG. We assume that this regime corresponds to normal *in vivo* conditions which we intended to model in this work.

Our central hypothesis is that the locomotor CPG has two functional levels: a half-centre RG and an intermediate PF network that distributes and coordinates the activities of multiple motoneurone populations under control of the RG (see Fig. 1). The schematic of the computational model explored in the present study is shown in Fig. 2*A*. To maintain the analogy with the experimental data in decerebrate cats, locomotion is initiated in the model by external tonic excitation (from the 'MLR') that is distributed among the excitatory neural populations of the CPG (RG and PF networks). The RG consists of two populations (RG-E and RG-F) of excitatory neurones with I_{NaP}-dependent pacemaker properties and mutual excitatory synaptic connections within and between them. Mutual inhibition between the RG-E and RG-F populations is mediated by the extensor and flexor inhibitory populations (Inrg-E and Inrg-F, respectively). In the absence of sensory input, the alternating busting activities of RG-E and RG-F populations define the extensor and flexor phases of the locomotor cycle, respectively. The activity of these populations is controlled by MLR excitatory drive, I_{NaP}-dependent subthreshold activation, mutual synaptic excitation within and between the RG-E and RG-F populations, and mutual inhibition mediated by the inhibitory Inrg-E and Inrg-F populations.

The PF network represents the second level of the CPG. According to our theoretical concept (see Fig. 1), this network should contain multiple PF populations controlled by the RG and provide phase-dependent activation of the corresponding groups of synergist motoneurone populations including the populations activating bifunctional muscles (acting across more than one joint). However in the reduced version of the model considered here, the PF network contains only two neural populations, PF-E and PF-F (see Fig. 2*A*). These populations receive tonic excitatory drive from the MLR, a weak excitatory input from the homonymous RG population, strong inhibition from the opposite RG population via a corresponding inhibitory population (Inrg-E or Inrg-F), and reciprocal inhibition from the opposite PF population via another inhibitory population (Inpf-F or Inpf-E) (see Fig. 2*A*).

Alternating activity of the RG populations results in periodic, alternating activity of the PF-E and PF-F populations. The PF populations transmit alternating rhythmic excitation to the extensor (Mn-E) and flexor (Mn-F) motoneurones and to inhibitory extensor (Ia-E) and flexor (Ia-F) interneurones (Fig. 2*A*). These Ia populations form a third level of reciprocal inhibition in the system. In the model they provide the rhythmic inhibition of motoneurone populations during the inactive phase of the step cycle (e.g. McCrea *et al.* 1980; Shefchyk & Jordan, 1985). According to our concept and in agreement with previous suggestions (Pratt & Jordan, 1987; Orlovsky *et al.* 1999), these 'local' reciprocal interactions between the direct antagonists sculpt the firing patterns of individual motoneurone pools. During normal locomotion (i.e. in the presence of afferent feedback), Ia interneurones also mediate reflex, group Ia, reciprocal inhibition of antagonist motoneurones (e.g. Lundberg, 1981; Jankowska, 1992). The model also includes populations of extensor and flexor Renshaw cells, R-E and R-F, respectively, which receive collateral excitatory input from the corresponding motoneurone populations (Mn-E and Mn-F) and provide feedback inhibition to the homonymous motoneurones. The circuitry of mutual inhibition between Ia-E and Ia-F populations, their inhibition by Renshaw cells and the mutual inhibition between Renshaw cells (see Fig. 2*A*) is in accord with the extensive work done on these interneurones in anaesthetized preparations (references in Jankowska, 1992). Unlike previous proposals (Miller

& Scott, 1977), the Ia and Renshaw populations do not participate in the maintenance or generation of rhythm (discussed in McCrea *et al.* 1980; Noga *et al.* 1987).

The weights of synaptic connections between the neural populations in our model are shown in Table 2 (see Appendix).

Figure 2*B* and *C* shows examples of computer simulations of locomotor rhythm generation and flexor and extensor motoneurone activity. Activity is represented by histograms of average neurone activity in the population. The basic locomotor rhythm is generated by the RG network. The alternating rhythmic bursts of the RG populations (top two traces of Fig. 2*B* and *C*) define the durations of extensor and flexor phases and hence the locomotor cycle period. An increase in MLR excitation to one RG population reduces the opposite phase duration (see below). In Fig. 2*B* the MLR drive to RG-E is stronger than that to RG-F, resulting in a longer duration extensor phase. In Fig. 2*C* increased drive to the RG-F population results in a flexor-dominated rhythm. Note that because of the separation of rhythm generating and motoneurone activating networks, the average firing rates of the motoneurone populations (two lower traces in Fig. 2*B* and *C*) are similar in the extensor- and flexor-dominated rhythms. In the reduced model considered here, in which the PF network consists of only two (extensor and flexor) populations reciprocally inhibiting each other, the activity of each PF population closely follows the activity of the corresponding RG population, and the activities of Ia inhibitory interneurones, motoneurones and Renshaw cells follow the activity of the corresponding (extensor or flexor) PF populations (see Fig. 2*B* and *C*). The rhythmic activity of Ia and Renshaw cells during fictive locomotion in the absence of sensory feedback has been previously demonstrated (Feldman & Orlovsky, 1975; McCrea *et al.* 1980; Pratt & Jordan, 1987).

Figure 3*A* illustrates the mechanisms for the locomotor rhythm generation induced by excitatory (MLR) drive to the CPG. The top three traces in this figure show,

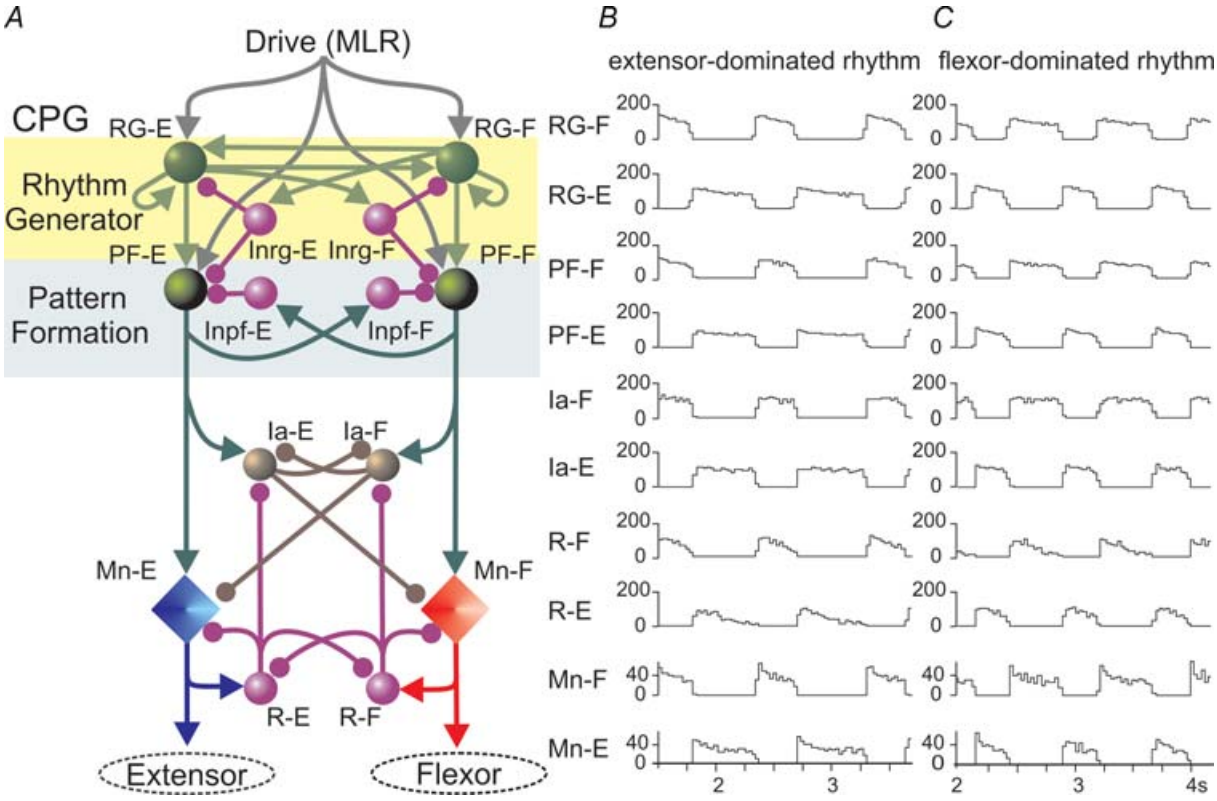

Figure 2. Model schematic and performance
A, schematic of the model. Populations of interneurones are represented by spheres. Excitatory and inhibitory synaptic connections are shown by arrows and small circles, respectively. Populations of motoneurones are represented by diamonds. See explanations in the text. *B* and *C*, model performance: the locomotor patterns generated by the model. Activity of each population is represented by a histogram of average firing frequency (number of spikes per second per neurone, bin = 30 ms). In *B*, the MLR drive to RG-E ($d_{rg\text{-}e}$) population is larger than to RG-F population ($d_{rg\text{-}f} = 0.43$; $d_{rg\text{-}e} = 0.5$), and the model generates a rhythm with a longer duration extensor phase ($T_E > T_F$). In *C*, the RG-F population receives a larger drive ($d_{rg\text{-}f} = 0.51$; $d_{rg\text{-}e} = 0.45$), and the model generates a flexion-dominated rhythm ($T_F > T_E$).

respectively: the average histogram of neurone activity in the RG-F population, the membrane potential trajectory of a single neurone from this population, and the change in the inactivation variable for NaP channel (h_{NaP}, see eqn (1)) in this neurone. The next three traces show the same variables for the RG-E population. The figure shows that during the phase of activity of each RG population, the I_{NaP} in neurones of this population is inactivating (see the slow reduction of h_{NaP}). The firing activity of the population is, however, maintained because of the supra-threshold activation of the fast sodium current. At the same time, there is an increasing excitability of the opposite (inactive) RG population due to the slowly increasing h_{NaP} (i.e. de-inactivation of I_{NaP}). At some point, the most excitable neurones in the previously silent RG population start firing. Mutual excitatory connections within the population further increase population excitability and synchronize neuronal activation. Firing in this RG population activates the corresponding Inrg inhibitory population (see traces for Inrg-F and Inrg-E populations in Fig. 3*A*) which reciprocally inhibits the previously active RG population and thus produces locomotor phase switching. Repetition of these processes produces alternating firing bursts of RG-E and RG-F populations and alternating activities of the extensor and flexor motoneurone populations (see Fig. 3*A*, bottom traces).

As described above, the generation of locomotor rhythm in the model results from a combination of I_{NaP}-dependent intrinsic mechanisms operating within each RG population, and the reciprocal inhibition between these populations. Specifically, the onset of bursts is critically dependent on intrinsic excitatory mechanisms (activation of I_{NaP}), whereas burst termination is mostly defined by the reciprocal inhibition. As a result, step cycle duration (locomotor period) is dependent upon (and may be regulated by) the external (MLR) drive to the RG and the reciprocal inhibition between the RG half-centres, as well as by the intrinsic characteristics of NaP channels in RG neurons. Figure 4*Aa* shows that locomotor period T decreases monotonically with an increase of MLR drive (consistent with the data of Sirota & Shik, 1973) and Fig. 4*Ab* shows the shortening of cycle period with an increase of reciprocal (mutual) inhibition between the RG half-centres. At the same time, T decreases monotonically with an increase of the maximal conductance of NaP channels in RG neurons (Fig. 4*Ac*) and increases linearly with an increase of the time constant for NaP channel inactivation (Fig. 4*Ad*).

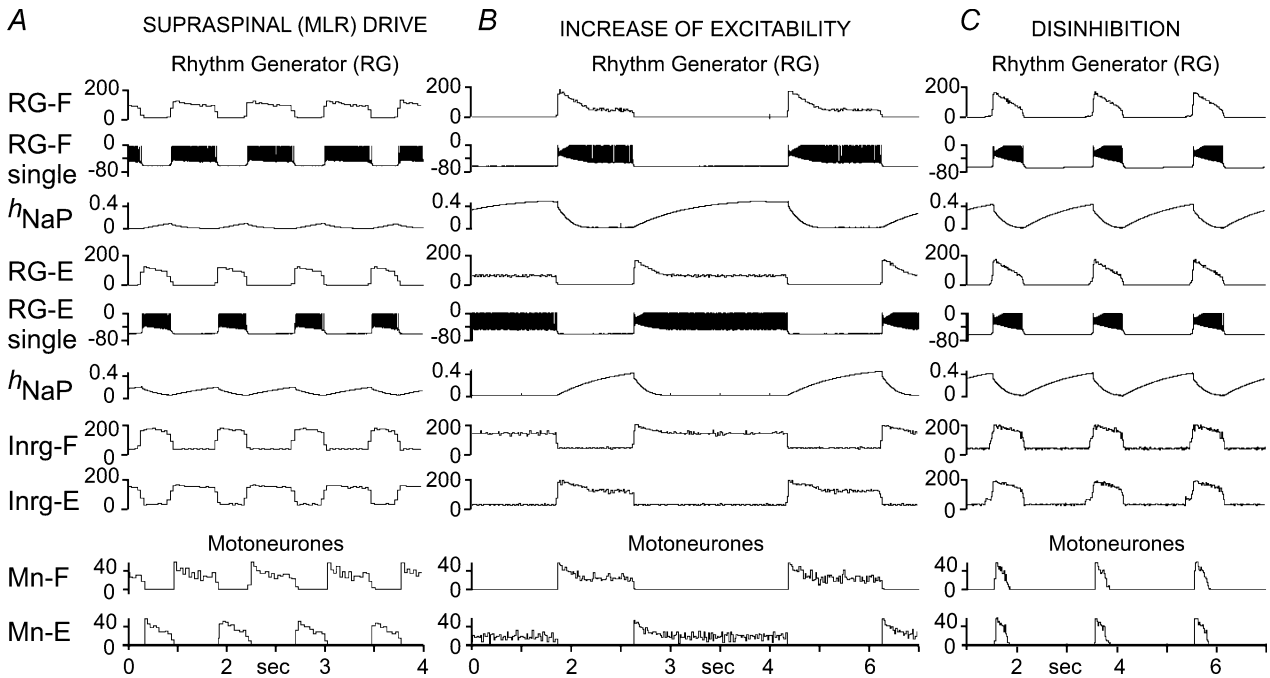

Figure 3. Rhythm generator performance under different conditions
A, generation of rhythmic activity evoked by supraspinal (MLR) drive to the RG ($d_{rg\text{-}f} = 0.51$; $d_{rg\text{-}e} = 0.45$). *B*, imitation of pharmacologically evoked rhythm in the model. The slow rhythmic activity was produced by an increase in excitability of the excitatory CPG populations (RGs and PFs) in the absence of external (MLR) drive. The increase of excitability was produced by a 6 mV depolarization of the average leakage reversal potential in all neurons of these populations. *C*, rhythmic activity produced in the model by disinhibiton. To simulate this behaviour, the weights of all inhibitory connections in the model were set to zero. Note synchronized rhythmic bursts of flexors and extensors. See details in the text.

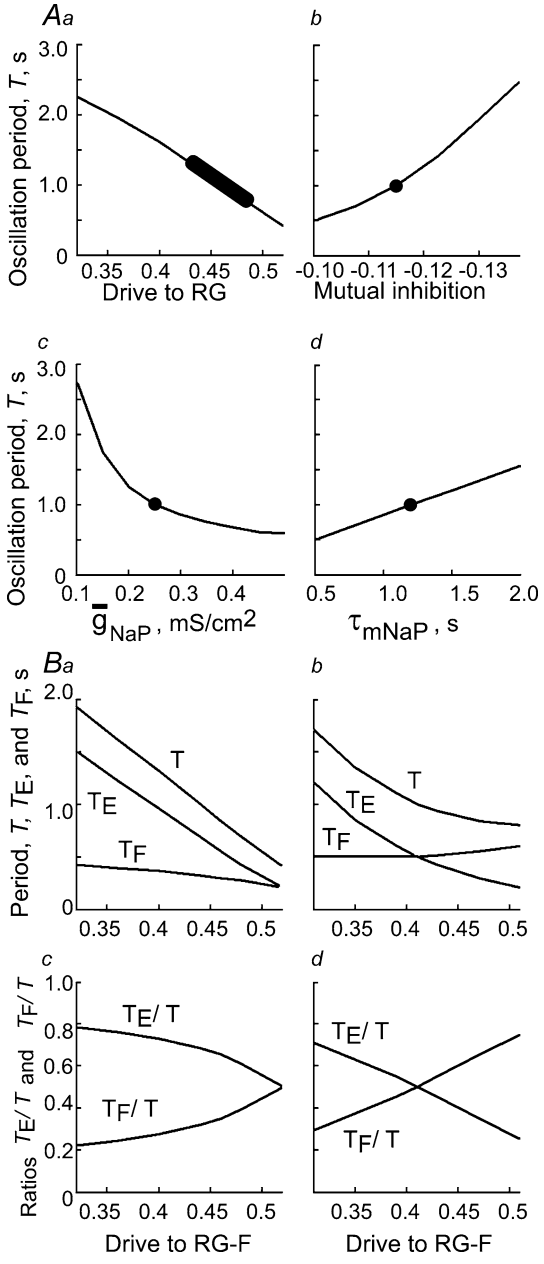

Figure 4. Durations of locomotor phases and step cycle and their dependence on model parameters

Aa, increased drive to the RG populations reduces step cycle duration (T) (a symmetrical case is considered: $d_{\text{rg-f}} = d_{\text{rg-e}} = 0.32$–$0.52$, see the horizontal axis). *Ab*, T monotonically increases with an increase in mutual inhibition between the RG populations. The increase of mutual inhibition was imposed by increasing the absolute value of the weight of inhibitory synaptic input from Inrg-E to RG-E and from Inrg-F to RG-F, which is indicated in the horizontal axis (see Fig. 2*A*). *Ac*, T monotonically decreases with an increase of the maximal conductance of NaP channels in RG neurons ($\bar{g}_{\text{NaP}}$) whose value is indicated in the horizontal axis. *Ad*, T linearly increases with an increasing maximal time constant for NaP channel inactivation ($\tau_{h\text{NaPmax}}$) indicated in the horizontal axis. In *Ab*–*Ad*, $d_{\text{rg-f}} = d_{\text{rg-e}} = 0.42$. *Ba*–*Bd*, the duration of step cycle and locomotor phases (T, T_{F} and T_{E} in *Ba* and *Bb*) and the relative durations of locomotor phases (T_{F}/T and T_{E}/T in *Bc* and *Bd*) produced by the model. MLR drive to the RG-E population was maintained constant ($d_{\text{rg-e}} = 0.52$ in *Ba* and *Bc*, and $d_{\text{rg-e}} = 0.41$ in *Bb* and *Bd*). Drive to RG-F ($d_{\text{rg-f}}$) was progressively increased from 0.32 to 0.52 in *Ba* and *Bc*, and from 0.31 to 0.51 in *Bb* and *Bd*, see the horizontal axes in *Ba*–*Bd*. Note that an increase of MLR drive to RG-F produces only small changes in the duration of the flexor phase, but substantially reduces the duration of the extensor phase and, correspondingly, the total duration of the step cycle.

In order to investigate the relative durations of the locomotor phases produced by the model, the MLR drive to one RG population (RG-E in Fig. 4*Ba*–*Bd*) was held constant (at 0.52 in Fig. 4*Ba* and *Bc* and at 0.41 in panels Fig. 4*Bb* and *Bd*), while the drive to the other RG population (RG-F) was progressively increased. Increasing MLR drive to one of the RG populations produced only small changes in the burst duration of that population and hence the duration of the corresponding locomotor phase (flexor in the example shown), but substantially reduced the duration of the opposite (extensor) phase and, correspondingly, the total duration of the step cycle. As seen in Fig. 4*Ba*–*Bd*, the model was able to generate MLR-evoked oscillations with step cycle period $T = 0.4$–2.5 s and ratio of phase durations to the period T_{F}/T (or T_{E}/T) $= 0.21$–0.79 that span the range of step cycle periods and phase durations observed during fictive locomotion in decerebrate cats (Yakovenko *et al.* 2005).

The results of our attempts to model oscillations under other conditions with no external MLR drive are shown in Fig. 3*B* and *C*. To model oscillations produced by monoamine neuromodulators, we suggest that neuromodulators increase the excitability of CPG excitatory populations (RGs and PFs). This suggestion is consistent with the data of Fedirchuk & Dai (2004) showing that monoamines (5-HT and noradrenaline) increase the excitability of spinal neurones in the rat via a 2–7 mV reduction in the threshold for action potential production. The mechanism of such an increase of excitability may also involve the inhibition of K^+ leak conductance (e.g. Kjaerulff & Kiehn, 2001; Perrier *et al.* 2003). To imitate the pharmacological increase of excitability in our model, the average leakage current reversal potential E_{L} was depolarized in all excitatory CPG neurone populations (RG and PF). Figure 3*B* shows that a depolarization of E_{L} by 6 mV in the model (in the absence of MLR drive) evoked slow locomotor-like oscillations with alternating flexor and extensor activities and $T = \sim 5$ s.

In our model the inhibitory interneurone populations, Inrg-F and Inrg-E, have a low level background activity between the RG-driven bursts. At rest this activity normally prevents CPG network operation in the absence of MLR drive. To simulate the oscillations evoked by blocking inhibitory transmission, the weights of all inhibitory connections in the model were set to zero. This produced spontaneous bursting activity in which flexor and extensor motoneurones are co-active (see Fig. 3*C*). Such activity

is qualitatively consistent with the experimental data obtained in the rat isolated spinal cord (Cowley & Schmidt, 1995; Bracci *et al.* 1996; Beato & Nistri, 1999) and during fictive locomotion in cats (Noga *et al.* 1993) using blockers of inhibitory synaptic transmission such as bicuculline and strychnine.

Figure 5 shows a comparison of modelled and experimental activities of flexor and extensor motoneurones during locomotion. The average spiking frequency of motoneurones in the model reaches 40 spikes s^{-1} (top and fourth traces in Fig. 5*A*) which is in general agreement with motoneurone firing during fictive locomotion in the cat (e.g. Brownstone *et al.* 1992). At the same time, because of the random distribution of motoneurone parameters within each population (specifically E_L), there are differences in the firing frequency, firing duration and recruitment of individual motoneurones (see raster plots, second and fifth traces in Fig. 5*A*). Similar to the intracellular recordings from single motoneurones during fictive locomotion, motoneurones in the model are hyperpolarized from their resting level (horizontal dashed lines in the third and bottom traces in Fig. 5*A*) during the phase in which they are inactive. Fig. 5*B* shows records from a bout of MLR-evoked fictive locomotion in a decerebrate cat plotted at the same time scale as the modelled results in Fig. 5*A*. The third and bottom traces are simultaneous intracellular recordings from a hip flexor (sartorius (Sart)) and a hip extensor (semimembranosus or anterior biceps (SmAB)) motoneurone, respectively. The remaining traces are population records (rectified, integrated neurograms) of flexor (hip, Sart, and ankle, tibialis anterior (TA)) and extensor (hip, SmAB, and ankle, medial gastrocnemius (MG)) motoneurone pool activities. A comparison of the left and right panels in Fig. 5 shows that the patterns of population activity of motoneurones and the traces of membrane potentials (and firing patterns) of single motoneurones in the model are qualitatively similar to those seen during fictive locomotion.

Modelling deletions

As described in the Introduction, deletions are brief failures in the alternating rhythmic activity of flexor and extensor motoneurones that occur spontaneously during fictive locomotion. During deletions the activity of multiple agonist motoneurone populations is missing for some period of time while the activity of their antagonists becomes tonic or continues to be rhythmic. Using our model, we suggest that deletions result from additional excitatory or inhibitory drive that changes the excitability of particular CPG populations.

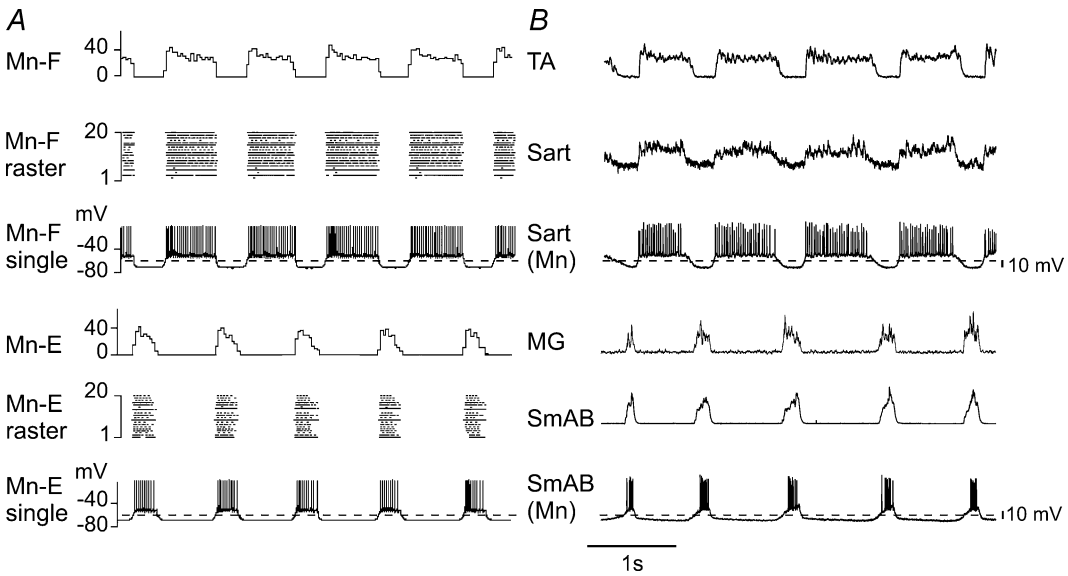

Figure 5. Motoneurone activities in the model and in the cat
A, examples of population activities of flexor and extensor motoneurones and membrane potential traces of single motoneurones in the model. Activities of flexor and extensor populations are represented by the average histograms (top trace for Mn-F and fourth trace for Mn-E) and raster plots (second trace for Mn-F and fifth trace for Mn-E). In both raster plots, the lines correspond to single motoneurones arranged by neurone numbers from 1 to 20, and the dots in each line represent spikes. Membrane potentials of one flexor and one extensor motoneurone are shown in third and bottom traces, respectively, with action potentials truncated at the level of −10 mV. In this simulation, the MLR drive to RG-F ($d_{rg\text{-}f}$) was 0.52 and to RG-E ($d_{rg\text{-}e}$) 0.46. *B*, records during MLR-evoked fictive locomotion showing electroneurogram (ENG) activity of ankle (tibialis anterior, TA) and hip (sartorius, Sart) flexors, ankle (medial gastrocnemius, MG) and hip (semimembranosus combined with anterior biceps, SmAB) extensors, and simultaneous intracellular recordings from a Sart and an SmAB motoneurone.

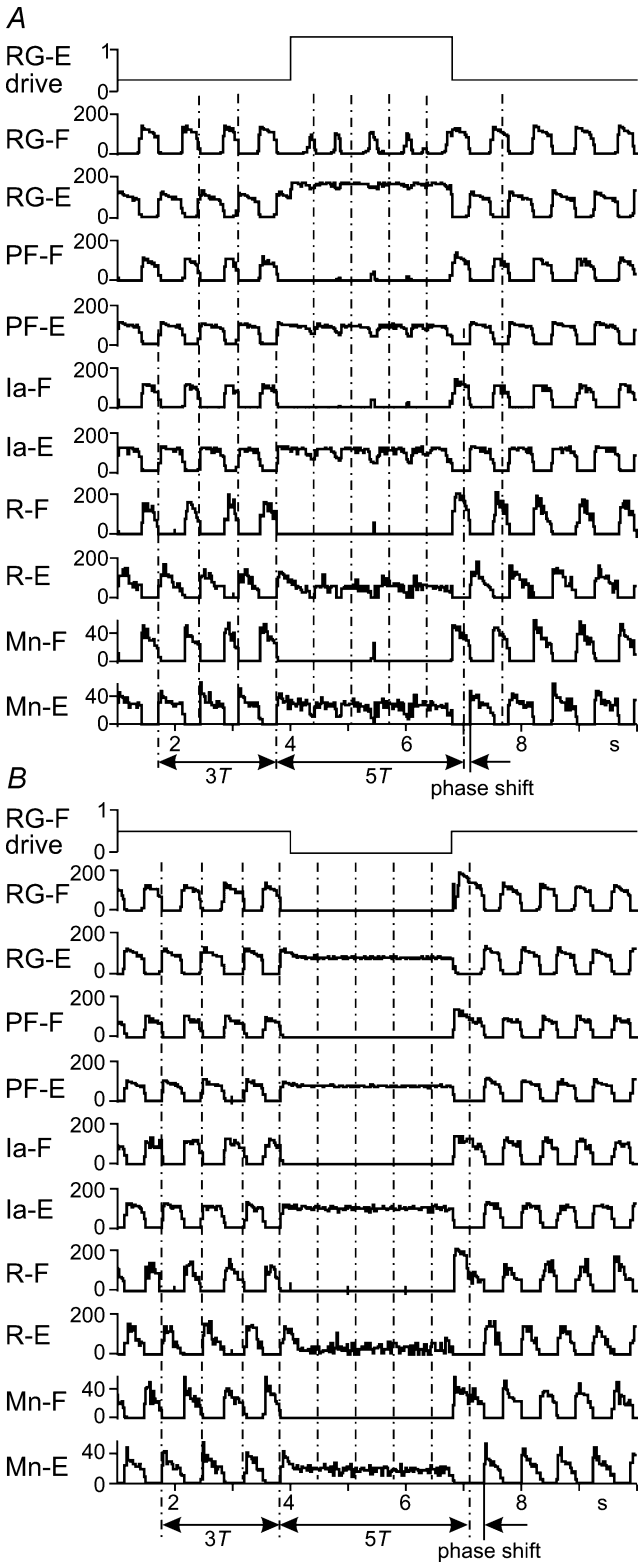

Figure 6. Simulations of 'resetting' deletions
A, an example of simulation of a resetting deletion. In this example, the deletion of flexor activity was produced by a temporary 400% increase in excitatory drive to the RG-E population (see the top trace). The increased drive changed RG-E population activity from phasic to sustained. Consequently during this additional excitation, all populations on the extensor side of the network (Ia-E, R-E and Mn-E) showed sustained activity, whereas all populations on the flexor side (Ia-F, R-F and Mn-F) were inhibited. As a result, at the motoneurone level (two bottom traces) there was a typical deletion of flexor motoneurone activity with a sustained activity of extensor motoneurones. *B*, in this example, the deletion of flexor activity was produced by a temporary removal of excitatory drive to the RG-F population (see the top trace). In both *A* and *B*, the vertical dotted lines are plotted at intervals representing the step cycle period preceding the deletion. These lines indicate where the onsets of extensor bursts would have occurred if there had been no deletion. Note that in both cases (*A* and *B*), when the applied 'perturbation' ends, the post-deletion rhythm re-appears with a phase shift in respect to the pre-deletion rhythm (see arrows at the bottom of each panel). In these simulations: $d_{rg\text{-}f} = 0.46$; $d_{rg\text{-}e} = 0.5$.

Figure 6*A* shows the results of our simulations in which an additional drive temporarily affects one of the RG populations. In this example, increased excitatory drive to RG-E (see the top trace in Fig. 6*A*) produces sustained activity in the RG-E half-centre and substantially reduces (or eliminates) activity in the opposite (RG-F) half-centre. As a result, at the motoneurone level (two bottom traces in Fig. 6*A*), there is a deletion of flexor motoneurone activity with a sustained activity of extensor motoneurones. A similar deletion of flexor motoneurone activity can be produced by temporarily reducing (or eliminating) excitatory drive to the flexor half-centre (see Fig. 6*B*). What is important to note in both Fig. 6*A* and *B* is that the onset and offset of the temporary change in RG excitability could occur at an arbitrary time with respect to the locomotor rhythm. Therefore, the post-deletion rhythm should be generally phase shifted or reset with respect to the pre-deletion rhythm (see Fig. 6*A* and *B*). Such 'resetting' deletions have been observed during fictive locomotion (Lafreniere-Roula & McCrea, 2005). An example is shown in Fig. 7*A*. In this example, the activity of all flexors (hip flexor – Sart, and ankle flexor –TA) was prolonged for some time period during which the extensor activity (hip extensor – SmAB, and ankle extensors – MG and lateral gastrocnemius combined with soleus (LGS)) was suppressed. This behaviour was closely reproduced in our model (see Fig. 7*B*) by applying a brief increase in excitatory drive to the RG-F population (top trace in Fig. 7*B*). In both the experimental and modelled cases there is an obvious phase shift of the post-deletion rhythm.

In contrast to the effects of altering excitability at the RG level, a temporary change in excitability of one of the PF populations produces a deletion without phase shift of the post-deletion rhythm. Figure 8*A* shows the effect of increased drive to the PF-E population (see the top trace). This increase results in sustained activity in the PF-E population and inhibition of activity in the opposite (PF-F) population. At the motoneurone level (two bottom traces in Fig. 8*A*), there is a deletion of flexor motoneurone activity with sustained activity of extensor motoneurones. Note, however, that there is a weak rhythmic modulation of

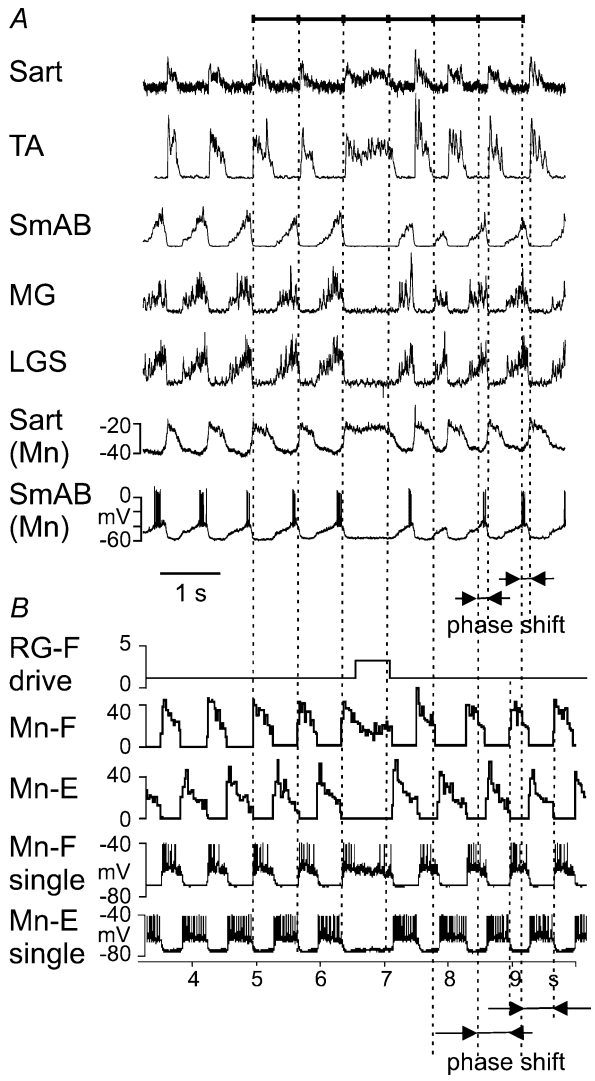

Figure 7. Example of 'resetting' deletion
A, a brief deletion of extensor activity that occurred during MLR-evoked fictive locomotion (Lafreniere-Roula & McCrea, 2005). The traces are rectified-integrated recordings from hip (sartorius, Sart) and ankle (tibialis anterior, TA) flexors, and hip (semimembranosus combined with anterior biceps, SmAB) and ankle (medial gastrocnemius (MG)) and lateral gastrocnemius combined with soleus, LGS) extensors. The bottom traces show simultaneous intracellular recordings from a Sart and a SmAB motoneurone. The vertical dotted lines are plotted at the intervals representing the average period calculated for the five step-cycle periods preceding the deletions. These lines indicate approximately where the onsets of flexor bursts would have occurred had there been no deletion. They show that the deletion is accompanied by an obvious phase shift of the post-deletion rhythm with respect to the pre-deletion rhythm (see arrows at the bottom). *B*, data from our simulation (similar to that in Fig. 6*A*) with the parameters (MLR drives) adjusted to fit phase durations in *A* ($d_{rg\text{-}f} = 0.48$; $d_{rg\text{-}e} = 0.5$). In this simulation, a deletion of extensor activity was produced by additional excitatory drive to the RG-F population (see the top trace). The two bottom traces show changes in the membrane potential of a single flexor and extensor motoneurone, respectively (action potentials truncated at −40 mV). As in the case of experimental recordings (see *A*), the 'perturbation' applied to the RG produced a resetting deletion accompanied by a shift in the phase of the post-deletion rhythm (see arrows at the bottom).

extensor motoneurone activity during the periods where flexor bursts 'should' have occurred as determined by continued rhythmic activity at the RG level.

If instead of increasing excitation to one of the excitatory PF populations the drive is reduced or eliminated, a different type of deletion occurs. This is shown in Fig. 8*B*, in which elimination of the excitatory drive to the PF-F population produced a deletion of flexor motoneurone activity accompanied by continued rhythmic activity of extensor motoneurones (see two bottom traces in Fig. 8*B*). Without a strong tonic excitatory drive to PF-F, the relatively weak phasic excitation from RG-F is not sufficient to overcome inhibition from Inrg-F. Therefore, the PF-F population and hence the Mn-F population remain inactive (a flexor deletion). On the other hand, the PF-E population receives both strong tonic (from MLR) and weak phasic (from RG-E) excitatory inputs and strong phasic inhibition (From Inrg-E). As a result, the activity in PF-E and hence Mn-E population remains rhythmic during the flexor deletion.

An important feature of the simulated deletions produced by alterations in PF network excitability (Fig. 8*A* and *B*) that distinguishes them from those produced by alterations in RG network excitability (Figs 6 and 7*B*) is the lack of resetting of the post-deletion rhythm. Because the locomotor rhythm is controlled by the RG, which is unaffected by the applied perturbations, the re-appearance of the rhythm after deletions occurs without shifting the phase of post-deletion oscillations. Such 'non-resetting' deletions do occur during fictive locomotion and are in fact more frequent than the 'resetting' type of deletion (see Lafreniere-Roula & McCrea, 2005).

Figure 9*Aa* and *Ab* shows examples of non-resetting deletions of flexor activity obtained during bouts of fictive locomotion. In Fig. 9*Aa* (data from Lafreniere-Roula & McCrea, 2005), the failure of hip (Sart) and ankle (extensor digitorum longus (EDL)) flexor motoneurone activation is accompanied by the continuous activity of extensors operating at the hip (SmAB), knee (quadriceps (Quad)) and ankle (Plantaris (Plant)). Note that flexor activity re-appears at the moments expected had the deletion not occured (see the fourth and sixth (from the left) vertical dashed lines). Note also that during some of the expected bursts there is a weak modulation of the sustained extensor motoneurone activity (marked by asterisk). Fig. 9*Ab* (M. Angel, P. Guertin, M.C. Perreault & D. McCrea, unpublished observations) shows the results of an experiment in which both ipsilateral and contralateral flexor and extensor activities were recorded. During the bout of fictive locomotion illustrated, there was no activity in the contralateral flexor and extensor nerves (see coTA and coMG traces). This non-resetting deletion of ipsilateral flexor activity (omitting two bursts in the iTA trace) was accompanied by a sustained firing of ipsilateral extensors (iAB and iLGS). This example shows that the

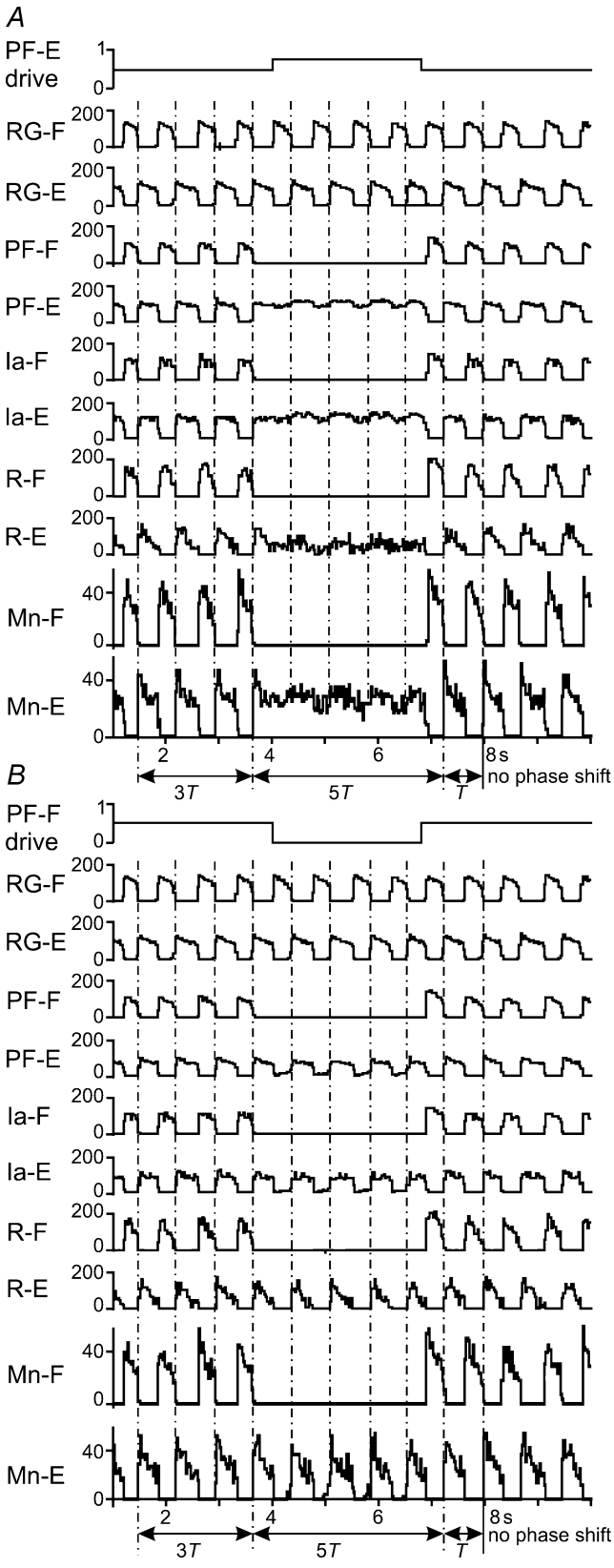

Figure 8. Simulation of 'non-resetting' deletions
A, an example of simulation of non-resetting deletion. The deletion of flexor activity was produced by a temporary 90% increase in excitatory drive to the PF-E population (see the top trace). This additional drive produced sustained PF-E population activity that inhibited the PF-F population. As a result, during the deletion there was sustained activity in all populations on the extensor side of the network (Ia-E, R-E and Mn-E), whereas all populations on the flexor side (Ia-F, R-F and Mn-F) were inhibited. At the motoneurone level (two bottom traces), there was a typical deletion of flexor motoneurone activity with a sustained activity of extensor motoneurones. *B*, an example of simulation of a non-resetting deletion with maintained rhythmic activity in antagonists. A temporary removal of excitatory drive to the PF-F population (see the top trace) stopped the activity of this population. Rhythmic activity was maintained, however, in the PF-E population because of the phasic inhibition provided by the RG-F population via the Inrg-E population (see Fig. 2*A*). As a result, at the motoneurone level (two bottom traces) there was a deletion of flexor motoneurone activity with maintained rhythmic activity of extensor motoneurones. As in Fig. 6, the vertical dotted lines in both panels are plotted at intervals representing the step cycle period preceding the deletion. These lines show that in both cases (*A* and *B*), the rhythm re-appeared after deletion without a phase shift with respect to the pre-deletion rhythm (see arrows at the bottom of each panels). In both simulations: $d_{rg\text{-}f} = 0.48$; $d_{rg\text{-}e} = 0.5$. Note that all changes (stepwise increase and decrease) of the total drive were applied in the middle of the ongoing phase to ensure that the timing of the post-deletion rhythm was controlled by rhythmic input from the RG.

maintenance of the phase of locomotor oscillations during non-resetting deletions is not dependent upon continued rhythm in the contralateral hindlimb. The activities shown in Fig. 9*Aa* and 9*Ab* were simulated in a manner similar to in the example shown in Fig. 8A by temporarily increasing excitatory drive to the PF-E population (see Fig. 9*Ba* and 9*Bb*). In both examples, the locomotor period (defined by neural activity at the RG level) was unaffected even though there was a failure to excite flexor motoneurones. The simulations show a rhythmic modulation of the sustained activity of extensor motoneurones (Mn-E) during flexor deletions that is similar to that observed in the extensor ENGs during fictive locomotion (e.g. see traces for SmAB, Quad, MG and Plant in Fig. 9*Aa*).

Figure 10*A* shows an example of a non-resetting deletion of extensor activity during fictive locomotion (from Lafreniere-Roula & McCrea, 2005). In this example, an unknown spontaneous perturbation caused the deletion of activity of extensor motoneurones operating at hip (SmAB) and ankle (gastrocnemius combined with soleus (GS) and Plant) accompanied by a sustained activity of flexor motoneurones (TA and peroneus longus (PerL)). The failure of flexor motoneurones to hyperpolarize during this period is illustrated in the intracellular record from a TA motoneurone (Fig. 10*A*, bottom trace). The re-appearance of extensor ENG activity (SmAB, GS and Plant) occurred at the time expected had the deletion not occurred. Note the hyperpolarization of the flexor (TA) motoneurone when extensor motoneurone activity re-appears following the deletion. This behaviour was simulated with our model by applying a temporary increase in total excitatory drive to the PF-F population

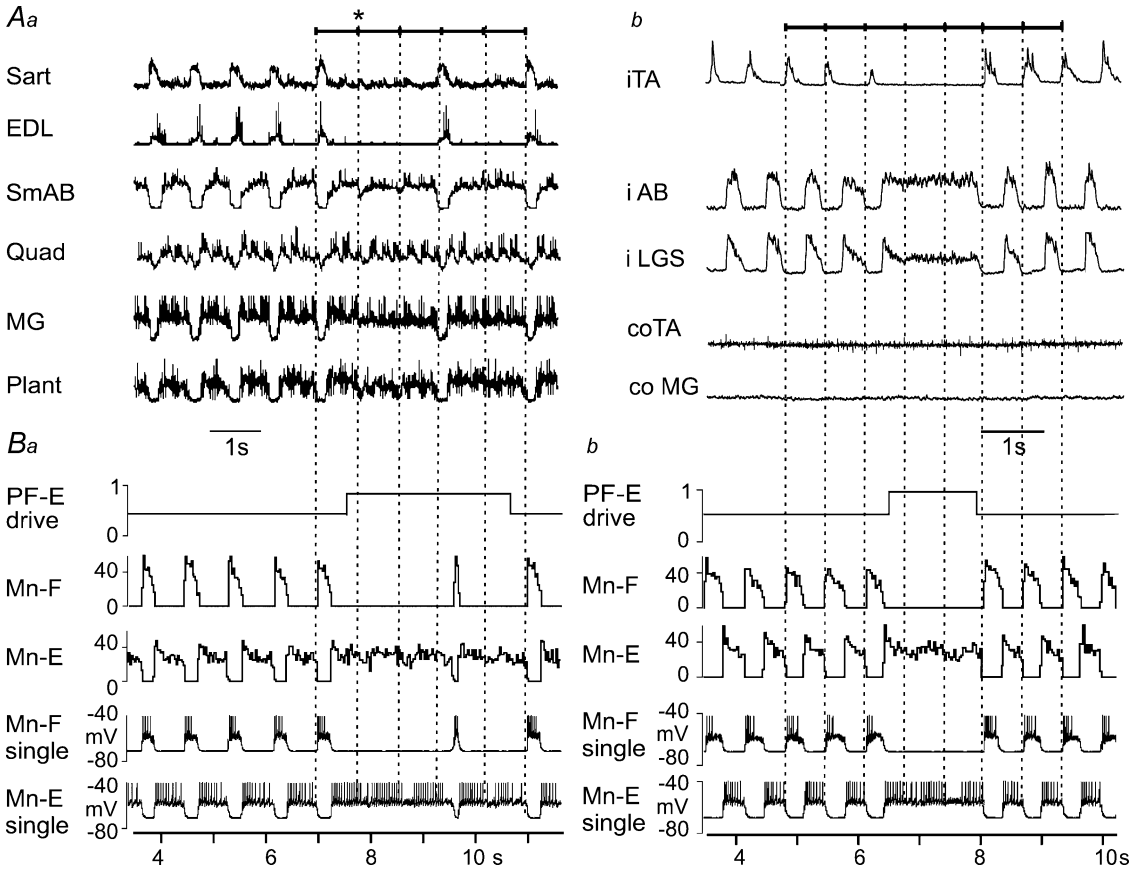

Figure 9. 'Non-resetting' deletions of flexor activity with a sustained activity of extensors
Aa, an example of deletion of flexor activity occurring during MLR-evoked fictive locomotion (Lafreniere-Roula & McCrea, 2005). The traces are rectified–integrated recordings from hindlimb flexors (hip – sartorius (Sart), and ankle – extensor digitorum longus (EDL)) and extensors (hip – semimembranosus combined with anterior biceps (SmAB), knee – quadriceps (Quad) and ankle – medial gastrocnemius (MG) and plantaris (Plant)). As in Fig. 7, the distance between the vertical dotted lines is the average step cycle period prior to the deletions. These lines indicate where the onsets of flexor bursts would have occurred if there had been no deletion. They show that the phase of the locomotor rhythm is maintained after the deletion. A weak modulation of the sustained extensor motoneurone activity is indicated (*). *Ab*, another example of deletion of flexor activity. An epoch of fictive locomotion is shown during which there was no contralateral (co) flexor and extensor activity (see coTA and coMG traces). The non-resetting deletion of ipsilateral flexor activity (in which two bursts in the iTA trace were omitted) was accompanied by a sustained firing of ipsilateral (i) extensors (iAB and iLGS). As in the example shown in *Aa*, the vertical dotted lines show that the phase of the locomotor rhythm is maintained after the deletion despite the absence of contralateral locomotor activity. *Ba*, data from our simulation (as in Fig. 8*A*) with the parameters (MLR drives) adjusted to fit phase durations in *Aa* ($d_{rg\text{-}f} = 0.44$; $d_{rg\text{-}e} = 0.55$). In this simulation, a deletion of flexor activity was produced by increased excitatory drive to the PF-E population (see the top trace). As in the experimental recordings in *Aa*, the phase of the locomotor rhythm is maintained after the deletion. The two bottom traces show changes in the membrane potential of single flexor and extensor motoneurones, respectively (action potentials truncated at −40 mV). In the experimentally observed deletion shown in *Aa*, first two flexor bursts are missing then one burst appears and then another is missing. To reproduce a similar pattern in the simulation, the drive to PF-E was increased to near threshold for reproducing the deletion (providing an 88% increase in total drive). Using a randomization process, the simulation was repeated until the data illustrated in *Ba* were obtained. Other deletion trials showed deletions of all four sequential flexor bursts or had flexor activity in one of the other deleted cycles. Note that during the deletion, the simulated flexor motoneurone (Mn-F) is hyperpolarized. The extensor motoneurone shows phasic modulation in its spiking without hyperpolarization, similar to that observed in ENGs of extensors (SmAB, Quad and Plant) in *Aa*. *Bb*, data from our simulation (similar to data in Fig. 8*A*) with the MLR drives adjusted to fit phase durations in *Ab* ($d_{rg\text{-}f} = 0.5$; $d_{rg\text{-}e} = 0.5$). The deletion of flexor activity was produced by an additional temporary excitatory drive to the PF-E population (see the top trace). As in the experimental recordings in *Ab*, the phase of the locomotor rhythm is maintained after the deletion.

(see Fig. 10*B*). This resulted in a striking similarity to the deletion occurring during fictive locomotion including the weak modulation of flexor activity at the point of expected extensor activity (marked by asterisks in Fig. 10*A*).

Our simulations demonstrate that individual motoneurones whose activity is 'deleted' are hyperpolarized during the deletion (see the second traces from the bottom in Fig. 9*Ba* and *Bb* and the bottom trace in Fig. 10*B*). In the model, this hyperpolarization is provided by the continuous inhibition from the antagonist Ia population. In contrast, individual motoneurones from the population active during the deletion show a modulation of firing but not a hyperpolarization (see bottom traces in Fig. 9*Ba* and *Bb* and fourth trace in Fig. 10*B*). These modelling results are consistent with the intracellular recordings of motoneurone activity during deletions (see Fig. 10*A*, bottom trace).

Figure 11*A* shows an example of a non-resetting deletion of agonist motoneurones with continued rhythmic activity of antagonists observed during fictive locomotion (from Lafreniere-Roula & McCrea, 2005). The failure of excitation of extensor motoneurones operating at the hip (SmAB) and ankle (MG and LGS) was accompanied by bursting of flexor motoneurones (hip flexor – Sart, and ankle flexors – TA and PerL). After the deletion, extensor activity re-appears without phase shift (i.e. similar to that during other non-resetting deletions). This behaviour could be simulated with our model (as in the example shown in Fig. 8*B*) by a temporary suppression of excitatory drive to the PF-E population (see Fig. 11*B*). Under these conditions, the model reproduced the deletion of activity of extensor motoneurones accompanied by continued bursting activity of the flexor motoneurone population. As in the experimental recordings (Fig. 11*A*), locomotor periods (defined by RG) remained unaffected when flexor motoneurone activity dropped out (Fig. 11*B*).

Discussion

The major hypothesis explored in this study is that the locomotor CPG has a two-level architecture consisting of a half-centre RG and a PF network (Figs 1 and 2*A*). Although some features of this architecture have been suggested previously (e.g. Koshland & Smith, 1989; Kriellaars *et al.* 1994), we are unaware of any formal consideration of the internal organization or modelling of network operation using such an architecture. The proposed two-level CPG architecture has several advantages. In particular, the separation of RG and PF networks permits independent control of rhythm generation at the RG level and patterns of motoneurone activity at the PF level. The present results show that the suggested CPG architecture can readily account for the resetting and non-resetting types of deletions observed during fictive locomotion in the cat (Lafreniere-Roula & McCrea, 2005). In the companion paper (Rybak *et al.* 2006) we also show that this two-level CPG structure can provide an explanation for the ability of afferent stimulation to control rhythm generation without changing the level of motoneurone activity (e.g. Kriellaars *et al.*

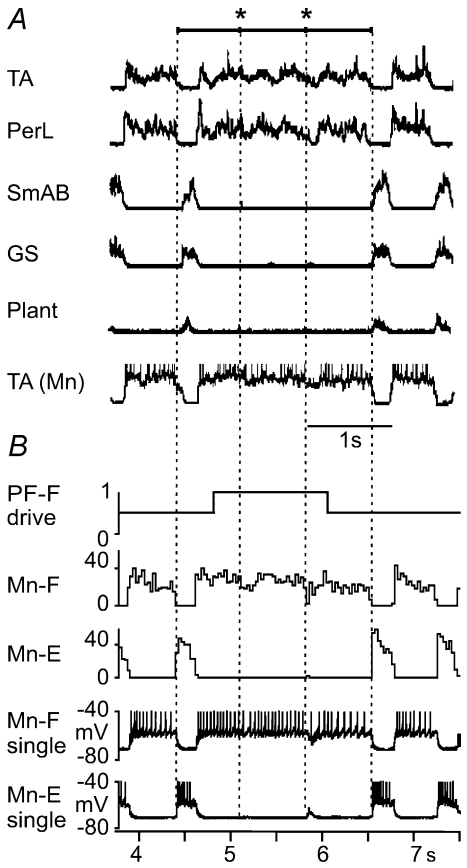

Figure 10. 'Non-resetting' deletion of extensor activity with a sustained activity of flexors
A, an example of a deletion of extensor activity during fictive locomotion. The recordings were made from ankle flexors (tibialis anterior, TA) and peroneus longus, PerL), and hip (semimembranosus combined with anterior biceps, SmAB) and ankle (gastrocnemius combined with soleus, GS, and plantaris, Plant) extensors (Lafreniere-Roula & McCrea, 2005). The vertical dotted lines, indicating where the onsets of extensor bursts would have occurred had there been no deletion, show that the phase of the locomotor rhythm is maintained after the deletion. The bottom trace is an intracellular recording from TA motoneurone. *B*, data from our simulation with the parameters (MLR drives) adjusted to fit phase durations in *A* ($d_{rg\text{-}f} = 0.62$; $d_{rg\text{-}e} = 0.44$). In this simulation, a deletion of extensor activity was produced by a 100% increase in excitatory drive to the PF-F population (see the top trace). As in the experimental recordings in *A*, the phase of the locomotor rhythm is maintained after deletion. The two bottom traces show changes in the membrane potential of single flexor and extensor motoneurones, respectively (action potentials truncated at −40 mV). Note that during the deletion the extensor motoneurone is hyperpolarized whereas the flexor motoneurone shows phasic modulation without an obvious hyperpolarization similar to that in an intracellular recording from TA motoneurone (see the bottom trace in *A*).

1994) and to control motoneurone activity without changing the rhythm (e.g. Guertin *et al.* 1995).

The half-centre concept and the two-level CPG architecture

In accord with the original Graham Brown-Lundberg half-centre model, our model employs flexor and extensor circuits that are organized symmetrically within the CPG. An alternative view is that the periodic inactivation of extensor bursts requires inhibition from a flexor half-centre whereas the inverse is not true (see Duysens *et al.* 2006). Evidence against this view includes the existence of spontaneous deletions of activity during fictive locomotion in both the flexors (e.g. see Fig. 9*Aa* and *Ab*) and extensors (e.g. Fig. 10*A*) that are both accompanied by sustained activity of the antagonists (Lafreniere-Roula & McCrea, 2005). Moreover, in the absence of proprioceptive feedback during MLR-evoked fictive locomotion, there can be a dominance in duration of either the flexor or the extensor phase (Yakovenko *et al.* 2005). Thus we suggest that although CPG can operate asymmetrically during normal locomotion (as a consequence of afferent feedback), its organization appears to be symmetrical for the generation of flexor and extensor motoneurone activities (see Duysens *et al.* 2006).

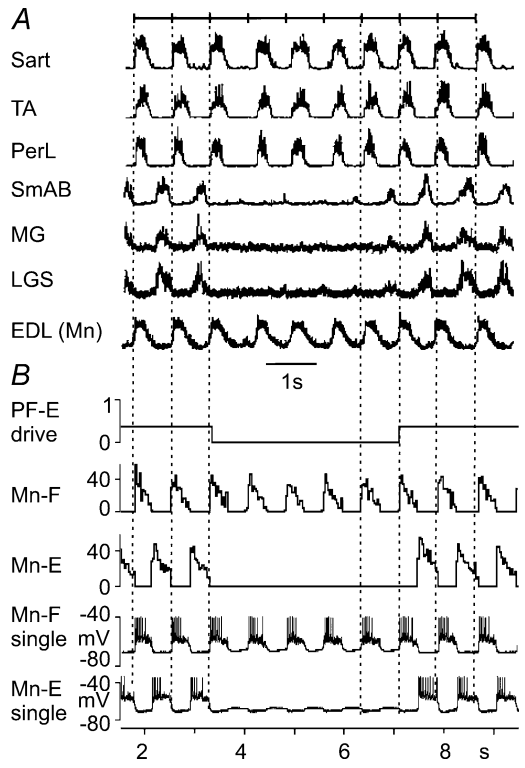

Figure 11. Example of a non-resetting deletion with maintained rhythmic activity of antagonist motoneurones
A, example of a deletion of extensor activity accompanied by continued rhythmic activity of flexor motoneurones (Lafreniere-Roula & McCrea, 2005). The recordings were made from hip (sartorius, Sart) and ankle (tibialis anterior, TA, and peroneus longus, PerL) flexors, and hip (semimembranosus combined with anterior biceps, SmAB) and ankle (medial gastrocnemius, MG, and lateral gastrocnemius combined with soleus, LGS) extensors. The bottom trace shows intracellular recording from an extensor digitorum longus (EDL) motoneurone that did not generate action potentials during fictive locomotion. The vertical dotted lines indicate where the termination of extensor bursts would have occurred if there had been no deletion. They show that the phase of the locomotor rhythm is maintained after deletion. *B*, data from our simulation (similar to data in Fig. 8*B*) with the MLR drives adjusted to fit phase durations in *A* ($d_{rg\text{-}f} = 0.46$; $d_{rg\text{-}e} = 0.48$). In this simulation, a deletion of flexor activity was produced by a temporary removal of excitatory drive to the PF-E population (see the top trace). Two bottom traces show membrane potentials of single flexor and extensor motoneurones, respectively (action potentials truncated at −45 mV). As in the experimental recordings in *A*, the phase of the locomotor rhythm did not change after deletion.

The idea that a mammalian CPG can contain separate RG and PF circuits was suggested in studies of the respiratory CPG (e.g. Rekling & Feldman, 1998; Feldman & McCrimmon, 1998; Smith *et al.* 2000), but was not commonly accepted and confirmed experimentally (e.g. see McCrimmon *et al.* 2000). The concept of the two-level organization of the locomotor CPG proposed here has been drawn explicitly from our experimental findings of non-resetting deletions occurring spontaneously during MLR-evoked fictive locomotion (Lafreniere-Roula & McCrea, 2005). Accordingly, we suggest that phase maintenance during non-resetting deletions occurs with changes in excitability that affect the PF but not the RG network. An alternative explanation is that activity in the contralateral limb or in the forelimbs maintains the phase during non-resetting deletions. While strong interactions between the limbs can influence step cycle timing in preparations with intact proprioceptive feedback, Fig. 9*Ab* illustrates that during fictive locomotion in immobilized cats, ipsilateral cycle timing during deletions can be maintained even in the absence of contralateral rhythmic activity. Of importance, cycle timing can also be maintained throughout deletions during fictive scratch where rhythmic activity in the other limbs is expected to be absent or very weak (Lafreniere-Roula & McCrea, 2005). While the possibility that contralateral or forelimb CPGs contribute to phase preservation during some deletions cannot be excluded, the evidence suggests that the circuitry controlling the ipsilateral hindlimb is itself able to maintain the phase of locomotor oscillations during deletions. We consider the frequent occurrence of non-resetting deletions as strong support for the concept of the two-level CPG proposed in this study.

As in the original Graham Brown-Lundberg half-centre model, we suggest a bipartite organization of the RG. One general difficulty with such an organization (discussed by Grillner, 1981; Stein & Smith, 1997) is that the classical one-level half-centre CPG cannot readily account for complex activities of different motoneurone pools

during fictive or real locomotion or during different locomotor tasks (Engberg & Lundberg, 1969; Perret & Cabelguen, 1980; Smith *et al.* 1998; Krouchev *et al.* 2006). One potential solution to this problem proposed by Grillner (1981) is that the CPG consists of multiple coupled oscillators or UBGs controlling motoneurones operating at each joint (see Edgerton *et al.* 1976; Grillner & Zangger, 1979; Stein, 1985; Stein & Smith, 1997). The UBG concept can potentially resolve many difficulties of a simple half-centre model (see Grillner, 1981). However, the UBG schematic in which a single network within each unit is responsible for both rhythm generation and motoneurone excitation appears to be principally unable to reproduce (or provide a reasonable explanation for) the maintenance of the phase of locomotor oscillations observed after non-resetting deletions or during afferent stimulation (see Introduction and accompanying paper Rybak *et al.* 2006). Further discussion of the UBG and the present concept of CPG organization is presented elsewhere (Lafreniere-Roula & McCrea, 2005).

Another solution of the problem is to maintain a bipartite organization of the RG but incorporate a more complicated intermediate PF network, operating between the rhythm generator and motoneurones (Perret & Cabelguen, 1980; Perret, 1983; Burke *et al.* 2001). This idea led to the two-level architecture of the locomotor CPG proposed here (see Fig. 1). The proposed two-level CPG includes a network of multiple PF populations operating at PF level. We believe that suitable interactions within the PF network and between the RG and PF networks can provide the generation and shaping of more complicated motoneurone activity including that of bifunctional motoneurones (see Chakrabarty *et al.* 2004), and overcome most of the limitations of the simple half-centre organization. In our opinion, a principal advantage of the UBG, namely the control of activity of subsets of motoneurones during locomotion, could also be accomplished within an organization composed of multiple PF networks of varying complexity.

It is important to notice that our model proposes three levels of reciprocity in the spinal circuitry: inhibitory interactions operating at the RG and PF levels and inhibition between antagonist motoneurones produced by populations of interneurones outside of the CPG *per se* and represented in the model by Ia interneurones. Recent evidence suggests that the rhythmic inhibition of motoneurones during locomotion involves interneurone populations in addition to the Ia interneurones depicted in the present model (Gosgnach *et al.* 2006). Regardless of their identity, additional control of motoneurone excitability by inhibitory interneurones involved in RG or PF networks would allow for the dissociation of rhythmic excitation and inhibition of motoneurones observed in some neonatal preparations (Hochman & Schmidt, 1998). In agreement with previous suggestions (Pratt & Jordan, 1987; Orlovsky *et al.* 1999), the 'local' reciprocal interactions via Ia interneurones provide an additional flexibility that could be manipulated (e.g. by afferent feedback) to shape the firing patterns of individual motoneurone pools. However, the reduced version of the model considered here, which contains only two PF populations and two motoneurone populations, cannot of course reproduce the full repertoire of motoneurone patterns recorded during fictive or real locomotion. This issue will be considered in future investigations using more complete computational models.

Modelling motoneurones, interneurones and the rhythm generating circuit

The intrinsic biophysical properties of different interneurone types in the mammalian spinal cord (such as the types of ionic channels and their voltage gating and temporal characteristics) have not been well characterized. This is especially true for the interneurones involved in CPG operation. Our models of interneurones do not represent realistic models of any particular spinal interneurones, but rather are generic models of the Hodgkin-Huxley type. At the same time, we believe that using such models gave us an opportunity to account for some non-linear properties of real neurones provided by the Hodgkin–Huxley formal descriptions.

Although more detailed multicompartment computational models of cat motoneurones are available (e.g. Dai *et al.* 2002), we used a two-compartment model (Booth *et al.* 1997) for computational efficiency. This model is able to reproduce the normal action potential firing behaviour observed in spinal motoneurones as well as a range of complex firing patterns, such as Ca^{2+}-dependent regenerative spiking and plateau potentials (Booth *et al.* 1997). Based on existing evidence (e.g. Lee & Heckman, 2001), we also incorporated persistent sodium channels in our model. A number of changes in motoneurone conductances during the transition from rest to fictive locomotion have been recently described in decerebrate cats. These include activation of voltage-dependent excitatory conductances, a reduction in the spike afterhyperpolarization and a lowering of voltage threshold for spike initiation (see Krawitz *et al.* 2001; Dai *et al.* 2002). We have not incorporated these changes in the present model. Instead, parameters were chosen to reproduce realistic firing rates and recruitment during locomotion in the simplified motoneurone models used. The present motoneurone model does, however, demonstrate realistic changes in the membrane potential and average firing frequency of single motoneurones and a range of individual motoneurone frequencies within the motoneurone populations (e.g. see Fig. 5).

Because the intrinsic neuronal mechanisms defining rhythmogenic properties of neurones comprising the

locomotor CPG are unknown, we chose to use a mechanism based on the persistent (slowly inactivating) I_{NaP} that has been shown to contribute to rhythmogenesis in other systems including respiratory rhythm generation (Butera *et al.* 1999*a*,*b*). The existing data, however, are certainly not sufficient to claim that the I_{NaP}-dependent mechanism employed in our model operates in the real locomotor CPG in the spinal cord. Other mechanisms based on different cellular properties, including those found in other preparations (see El Manira *et al.* 1994; Büschges *et al.* 2000; Grillner *et al.* 2001; Butt *et al.* 2002; Grillner & Wallén, 2002; Grillner, 2003), may be essential to the generation of locomotor rhythm in adult mammals.

We suggest that the hypothesized two-level architecture of the locomotor CPG proposed in our model has merit regardless of the particular cellular rhythmogenic mechanism employed in the model. An intrinsic excitatory rhythmogenic mechanism such as I_{NaP} is, however, critical to the generation of pharmacologically evoked rhythms (Fig. 3*B*) and the synchronized rhythmic activity of flexors and extensors when inhibition is blocked (Fig. 3*C*). Thus the generation of locomotor rhythm in our model is based on RG half-centres containing populations of neurons with intrinsic rhythmogenic properties allowing each half-centre, under certain conditions, to generate rhythmic activity on its own.

At the same time, the locomotor rhythm and pattern generated in our model is strongly dependent on the reciprocal inhibition between the RG half-centres (e.g. see Fig. 4*Ab*). Moreover, this inhibition plays a crucial role in the coupling of locomotor phases, phase switching, and hence in the regulation of the duration of locomotor phases and step cycle. A combination of the intrinsic I_{NaP}-dependent properties of RG neurones with the reciprocal inhibition between the RG half-centres allowed our model to simulate MLR-evoked locomotor oscillations with a realistic range of step cycle durations and ratio of one phase duration to the period (Fig. 4*Ba* and *Bb*). Therefore, we believe that regardless of the intrinsic rhythmogenic mechanisms operating in spinal neurons comprising the CPG, the reciprocal inhibitory interactions between the RG half-centres are extremely important for locomotor rhythm generation. Moreover, we think that reciprocal inhibitory interactions between functionally antagonistic neural populations at all levels, from the level of rhythm generator to the level of local, Ia-mediated interactions between direct antagonists, are essential for coordination and shaping the locomotor pattern.

Deletions

The CPG model described here evolved primarily from observations of deletions in motoneurone activity occurring spontaneously during MLR-evoked fictive locomotion in adult decerebrate cats (Lafreniere-Roula & McCrea, 2005). The major findings of that experimental study were that: (1) deletions of flexor or extensor activities are accompanied by either sustained (see examples in Figs 9*Aa* and 9*Ab* and 10*A*) or rhythmic (Fig. 11*A*) activity in antagonists; (2) deletions occur simultaneously in distal and proximal motoneurone pools; and (3) the majority of deletions are characterized by a maintenance of the phase of the post-deletion rhythm (Figs 9*Aa* and 9*Ab*, 10*A* and 11*A*). The two-level CPG architecture (with RG and PF levels, see Figs 1 and 2*A*) permits CPG operation with an unperturbed performance of the RG circuit when the motoneurone activations are altered by disturbances at the PF level. The incorporation of a PF network with reciprocal inhibition between the PF populations providing excitation to multiple groups of synergistic motoneurone pools, allows the model to reproduce and explain almost all of the experimental findings concerning deletions (Lafreniere-Roula & McCrea, 2005).

It is commonly accepted that reciprocal inhibition is necessary for the coordination of flexor and extensor motoneurone activities. This concept has been expressed as a 'reciprocity module' in which the excitation of antagonists is strictly coupled to inhibition of antagonists by specific interactions among Ia interneurones, Renshaw cells and motoneurones (Jordan, 1991). Studies of deletions provide additional experimental support for such an organization by showing that the reciprocal hyperpolarization of antagonist motoneurones observed during normal fictive behaviours is usually maintained during deletions (see Jordan, 1991; Lafreniere-Roula & McCrea, 2005). The present model incorporating a single reciprocity module shows that deletions of agonist activity are accompanied by a reduced hyperpolarization of antagonist motoneurones (see Figs 9*Ba* and *Bb*, and 10*B*).

Our modelling results give rise to the following hypotheses: (1) resetting deletions observed during fictive locomotion, that are associated with a phase shift in the post-deletion rhythm (as in Fig. 7*A*), result from spontaneous perturbations that change the excitability of one of the RG half-centres (see Figs 6*A* and 7*B*); (2) non-resetting deletions, characterized by the maintenance of the phase of the post-deletion rhythm (similar to those shown in Figs 9*Aa* and *Ab*, 10*A* and 11*A*), result from perturbations that do not affect the RG but instead change the excitability of one of the PF populations (see Figs 8*A* and *B*, 9*Ba* and *Bb*, 10*B* and 11*B*); (3) non-resetting deletions of motoneurone activity accompanied by a sustained activity of antagonists (e.g. shown in Figs 9*Aa* and *Ab*, and 10*A*) are produced by spontaneous perturbations increasing the excitability of the PF population projecting to the motoneurones with sustained activity during deletion (see Figs 8*A*, 9*Ba* and *Bb*, and 10*B*). In contrast, non-resetting deletions accompanied by continued rhythmic activity of antagonists (as in Fig. 11*A*) result from a spontaneous

Table 1. Steady-state activation and inactivation variables and time constants for voltage-dependent ionic channels

Ionic channels	$m_\infty(V)$, V is in mV $h_\infty(V)$, V is in mV	$\tau_m(V)$, ms $\tau_h(V)$, ms
Na^+	$m_{\infty Na} = (1 + \exp(-(V + 35)/7.8))^{-1}$ $h_{\infty Na} = (1 + \exp((V + 55)/7))^{-1}$	$\tau_{mNa} = 0$ $\tau_{hNa} = 30/(\exp((V + 50)/15) + \exp(-(V + 50)/16))$
Na_P^+	$m_{\infty NaP} = (1 + \exp(-(V + 47.1)/3.1))^{-1}$ $h_{\infty NaP} = (1 + \exp((V + 59)/8))^{-1}$	$\tau_{mNaP} = 0$ $\tau_{hNaP} = \tau_{hNaPmax}/\cosh(V + 59)/16)$, $\tau_{hNaPmax} = 1200$
K^+	$m_{\infty K} = (1 + \exp(-(V + 28)/15))^{-1}$ $h_K = 1$	$\tau_{mK} = 7/(\exp((V + 40)/40) + \exp((—V + 40)/50))$
Ca_N^{2+}	$m_{\infty CaN} = (1 + \exp(-(V + 30)/5))^{-1}$ $h_{\infty CaN} = (1 + \exp((V + 45)/5))^{-1}$	$\tau_{mCaN} = 4$ $\tau_{hCaN} = 40$
Ca_L^{2+}	$m_{\infty CaL} = (1 + \exp(-(V + 40)/7))^{-1}$ $h_{CaL} = 1$	$\tau_{mCaL} = 40$

All expressions and parameters, except those for the Na_P^+ channel, are taken from Booth *et al.* (1997). The expressions for the Na_P^+ channel are from Rybak *et al.* (2003).

decrease in excitability of the PF populations projecting to the motoneurones whose activity is 'deleted' (see Figs 8*B* and 11*B*).

Our analysis shows that in order for the model to operate properly, the mutual inhibition between the RG populations should be stronger than that between the PF populations. Accordingly, a much stronger perturbation is required to produce a resetting deletion at the RG level than to affect the PF circuit and produce a non-resetting deletion (see figure legends for Fig. 6*A* and Fig. 8*A* and compare the top traces in these figures). This might explain why non-resetting deletions occur more frequently during fictive locomotion than resetting deletions (Lafreniere-Roula & McCrea, 2005). Another feature of the model is that a deletion that silences activity in the longer duration locomotor phase requires a much greater increase in the excitability of the antagonistic PF population than a deletion affecting the shorter duration locomotor phase. This is consistent with the observation that most deletions during fictive locomotion occur in motoneurones active in the shorter duration locomotor phase (whether this shorter phase is flexion or extension).

Some modelling predictions

In this paper we have presented a simplified model of the spinal cord circuitry organization that reproduces and offers explanations for spontaneous deletions of motoneurone activity occurring with and without a resetting of the locomotor pattern. One immediate application of the present model is the formulation of criteria for the functional identification of new classes of spinal interneurones involved in the locomotor pattern generation. Based on our model, we suggest that the neurones comprising the RG may be identified in fictive locomotion preparations using the following criteria. These neurones should (1) receive excitation from the MLR region, (2) demonstrate rhythmic activity during fictive locomotion that persists during non-resetting deletions and (3) not be monosynaptically coupled to motoneurones. In contrast, the neurones comprising the PF network should (1) demonstrate rhythmic activity during fictive locomotion that fails during deletion episodes and (2) produce monosynaptic EPSPs in synergist motoneurones.

Appendix

General model parameters*

$$E_{Na} = 55\ \text{mV}; \quad E_K = -80\ \text{mV}; \quad E_{Ca} = 80\ \text{mV};$$
$$C = 1\ \mu\text{F cm}^{-2}.$$

Parameters of synapses

$$E_{SynE} = -10\ \text{mV}; \quad E_{SynI} = -70\ \text{mV};$$
$$\bar{g}_E = 0.05\ \text{mS cm}^{-2}; \quad \bar{g}_I = 0.05\ \text{mS cm}^{-2};$$
$$\bar{g}_{Ed} = 0.05\ \text{mS cm}^{-2}; \quad \bar{g}_{Id} = 0.05\ \text{mS cm}^{-2};$$
$$\tau_{SynE} = 5\ \text{ms}; \quad \tau_{SynI} = 5\ \text{ms}.$$

Neurone parameters

RG neurones:

$$\bar{g}_{Na} = 30\ \text{mS cm}^{-2}; \quad \bar{g}_{NaP} = 0.25\ \text{mS cm}^{-2};$$
$$\bar{g}_K = 1\ \text{mS cm}^{-2}; \quad g_L = 0.1\ \text{mS cm}^{-2};$$
$$E_L = -64.0 \pm 0.64\ \text{mV}.$$

Table 2 . Weights of synaptic connections in the network

Target population	Source population or drive (weight of synaptic input to one neurone)
RG-E	MLR (1); RG-E (0.0125); RG-F (0.0125); Inrg-E (−0.115)
RG-F	MLR (1); RG-E (0.0125); RG-F (0.0125); Inrg-F (−0.115)
Inrg-E	RG-F (0.45)
Inrg-F	RG-E (0.45)
PF-E	MLR (1); RG-E (0.0075); Inrg-E (−0.05); Inpf-E (−0.35)
PF-F	MLR (1); RG-F (0.0075); Inrg-F (−0.05); Inpf-F (−0.35)
Inpf-E	PF-F (0.2)
Inpf-F	PF-E (0.2)
Ia-E	PF-E (0.4); Ia-F (−0.1); R-E (−0.1)
Ia-F	PF-F (0.4); Ia-F (−0.1); R-F (−0.1)
R-E	Mn-E (0.25); R-F (−0.1)
R-F	Mn-F (0.25); R-E (−0.1)
Mn-E	PF-E (0.5); Ia-F (−0.6); R-E (−0.2)
Mn-F	PF-F (0.5); Ia-E (−0.6); R-F (−0.2)

Values in brackets represent relative weights of synaptic inputs from the corresponding source populations (w_{ji}) or drives (w_{dmi}), see Eqn. (10). MLR drives to PF-E and PF-F ($d_{pf\text{-}e} = d_{pf\text{-}f}$) = 0.5 for MLR drives to RG-E and RG-F ($d_{rg\text{-}e}$ and $d_{rg\text{-}f}$) see figure legends.

PF neurones:

$$\bar{g}_{Na} = 30 \text{ mS cm}^{-2}; \quad \bar{g}_{NaP} = 0.1 \text{ mS cm}^{-2};$$
$$\bar{g}_{K} = 1.2 \text{ mS cm}^{-2}; \quad g_{L} = 0.1 \text{ mS cm}^{-2};$$
$$E_{L} = -64.0 \pm 0.64 \text{ mV}.$$

Motoneurones*:

$$\bar{g}_{Na(S)} = 120 \text{ mS cm}^{-2}; \quad \bar{g}_{K(S)} = 100 \text{ mS cm}^{-2};$$
$$\bar{g}_{CaN(S)} = 14 \text{ mS cm}^{-2}; \quad \bar{g}_{K,Ca(S)} = 5 \text{ mS cm}^{-2}$$

$$g_{L(S)} = 0.51 \text{ mS cm}^{-2}; \quad E_{L(S)} = -65.0 \pm 6.5 \text{ mV};$$

$$\bar{g}_{CaN(D)} = 0.3 \text{ mS cm}^{-2}; \quad \bar{g}_{CaL(D)} = 0.33 \text{ mS cm}^{-2};$$
$$\bar{g}_{K,Ca(D)} = 1.1 \text{ mS cm}^{-2}; \quad \bar{g}_{NaP(D)} = 0.10 \text{ mS cm}^{-2};$$

$$g_{L(D)} = 0.51 \text{ mS cm}^{-2}; \quad E_{L(D)} = -65.0 \pm 3.25 \text{ mV};$$

$$g_{C} = 0.1 \text{ mS cm}^{-2}; \quad p = 0.1; \quad f = 0.01;$$
$$\alpha = 0.0009 \text{ mol C}^{-1} \ \mu\text{m}^{-1}; \quad k_{Ca} = 2 \text{ ms}^{-1};$$
$$K_{d} = 0.2 \ \mu\text{M}.$$

Other interneurones*:

$$\bar{g}_{Na} = 120 \text{ mS cm}^{-2}; \quad \bar{g}_{K} = 100 \text{ mS cm}^{-2};$$
$$g_{L} = 0.51 \text{ mS cm}^{-2};$$

$E_{L} =$
-64.0 ± 3.2 mV (for all interneurones except Inrg)
and
$E_{L} = 57.5 \pm 2.875$ mV(for Inrg).

The parameters indicated by * (except for E_{L}) are taken from Booth *et al.* (1997). To provide heterogeneity of neurones within neural populations, the value of E_{L} was randomly assigned from normal distributions (see mean values ± S.D.).

References

Beato M & Nistri A (1999). Interaction between disinhibited bursting and fictive locomotor patterns in the rat isolated spinal cord. *J Neurophysiol* **82**, 2029–2038.

Booth V, Rinzel J & Kiehn O (1997). Compartmental model of vertebrate motoneurons for Ca^{2+}-dependent spiking and plateau potentials under pharmacological treatment. *J Neurophysiol* **78**, 3371–3385.

Bracci E, Ballerini L & Nistri A (1996). Localization of rhythmogenic networks responsible for spontaneous bursts induced by strychnine and bicuculline in the rat isolated spinal cord. *J Neurosci* **16**, 7063–7076.

Brownstone RM, Jordan LM, Kriellaars DJ, Noga BR & Shefchyk SJ (1992). On the regulation of repetitive firing in lumbar motoneurones during fictive locomotion in the cat. *Exp Brain Res* **90**, 441–455.

Burke RE, Degtyarenko AM & Simon ES (2001). Patterns of locomotor drive to motoneurons and last-order interneurons: clues to the structure of the CPG. *J Neurophysiol* **86**, 447–462.

Büschges A, Wikstrom MA, Grillner S & El Manira A (2000). Roles of high-voltage activated calcium channel subtypes in a vertebrate spinal locomotor network. *J Neurophysiol* **84**, 2758–2766.

Butera RJ, Rinzel JR & Smith JC (1999*a*). Models of respiratory rhythm generation in the pre-Bötzinger complex. I. Bursting pacemaker neurons. *J Neurophysiol* **82**, 382–397.

Butera RJ, Rinzel JR & Smith JC (1999*b*). Models of respiratory rhythm generation in the pre-Bötzinger complex. II. Populations of coupled pacemaker neurons. *J Neurophysiol* **82**, 398–415.

Butt SJB, Harris-Warrick RM & Kiehn O (2002). Firing properties of identified interneuron populations in the mammalian hindlimb central pattern generator. *J Neurosci* **22**, 9961–9971.

Chakrabarty S, Rybak IA & McCrea DA (2004). Modelling the variety of activation patterns of bifunctional hindlimb motoneurons during fictive locomotion. *Abstr Soc Neurosci* 883.2.

Cowley KC & Schmidt BJ (1995). Effects of inhibitory amino acid antagonists on reciprocal inhibitory interactions during rhythmic motor activity in the in vitro neonatal rat spinal cord. *J Neurophysiol* **74**, 1109–1117.

Dai Y, Jones KE, Fedirchuk B, McCrea DA & Jordan LM (2002). A modelling study of locomotion-induced hyperpolarization of voltage threshold in cat lumbar motoneurones. *J Physiol* **544**, 521–536.

Darbon P, Yvon C, Legrand JC & Streit J (2004). INaP underlies intrinsic spiking and rhythm generation in networks of cultured rat spinal cord neurons. *Eur J Neurosci* **20**, 976–988.

Del Negro CA, Koshiya N, Butera RJ & Smith JC (2002). Persistent sodium current, membrane properties and bursting behavior of pre-Bötzinger complex inspiratory neurons *in vitro*. *J Neurophysiol* **88**, 2242–2250.

Duysens J (1977). Reflex control locomotion as revealed by stimulation of cutaneous afferents in spontaneously walking premammillary cats. *J Neurophysiol* **40**, 737–751.

Duysens J, McCrea D & Lafreniere-Roula M (2006). How deletions in a model could help explain deletions in the laboratory. *J Neurophysiol* **95**, 562–565.

Edgerton VR, Grillner S, Sjostrom A & Zangger P (1976). Central generation of locomotion in vertebrates. In *Neural Control of Locomotion*, ed. Herman RM, Grillner S, Stein PSG & Stuart DG, pp. 439–464. Plenum Press, New York.

El Manira A, Tegner J & Grillner S (1994). Calcium-dependent potassium channels play a critical role for burst termination in the locomotor network in lamprey. *J Neurophysiol* **72**, 1852–1861.

Engberg I & Lundberg A (1969). An electromyographic analysis of muscular activity in the hindlimb of the cat during unrestrained locomotion. *Acta Physiol Scand* **75**, 614–630.

Fedirchuk B & Dai Y (2004). Monoamines increase the excitability of spinal neurones in the neonatal rat by hyperpolarizing the threshold for action potential production. *J Physiol* **557**, 355–361.

Feldman AG & Orlovsky GN (1975). Activity of interneurons mediating reciprocal 1a inhibition during locomotion. *Brain Res* **84**, 181–194.

Feldman JL & McCrimmon DR (1998). Neural control of breathing. In *Fundamental Neuroscience*, ed. Bloom FE, Landis SC, Roberts JL, Squire LC & Zigmond MJ, chap. 40, pp. 1063–1090. Academic Press, New York.

Forssberg H, Grillner S, Halbertsma J & Rossignol S (1980). The locomotion of the low spinal cat. II. Interlimb coordination. *Acta Physiol Scand* **108**, 289–295.

Gosgnach S, Lanuza GM, Butt SJ, Saueressig H, Zhang Y, Velasquez T, Riethmacher D, Callaway EM, Kiehn O & Goulding M (2006). V1 spinal neurons regulate the speed of vertebrate locomotor outputs. *Nature* **440**, 215–219.

Graham Brown T (1911). The intrinsic factors in the act of progression in the mammal. *Proc R Soc Lond B Biol Sci* **84**, 308–319.

Graham Brown T (1914). On the fundamental activity of the nervous centres: together with an analysis of the conditioning of rhythmic activity in progression, and a theory of the evolution of function in the nervous system. *J Physiol* **48**, 18–41.

Grillner S (1981). Control of locomotion in bipeds, tetrapods, and fish. In *Handbook of Physiology. The Nervous System*. Motor Control sect.1, vol II, ed. Brookhart JM & Mountcastle VB, pp. 1179–1236. American Physiological Society, Bethesda.

Grillner S (2003). The motor infrastructure: from ion channels to neuronal networks. *Nat Rev Neurosci* **4**, 573–586.

Grillner S & Wallén P (2002). Cellular bases of a vertebrate locomotor system-steering, intersegmental and segmental co-ordination and sensory control. *Brain Res Rev* **40**, 92–106.

Grillner S, Wallén P, Hill R, Cangiano L & El Manira A (2001). Ion channels of importance for the locomotor pattern generation in the lamprey brainstem-spinal cord. *J Physiol* **533**, 23–30.

Grillner S & Zangger P (1979). On the central generation of locomotion in the low spinal cat. *Exp Brain Res* **34**, 241–261.

Guertin P, Angel MJ, Perreault M-C & McCrea DA (1995). Ankle extensor group I afferents excite extensors throughout the hindlimb during fictive locomotion in the cat. *J Physiol* **487**, 197–209.

Hochman S & Schmidt BJ (1998). Whole cell recordings of lumbar motoneurons during locomotor-like activity in the in vitro neonatal rat spinal cord. *J Neurophysiol* **79**, 743–752.

Jankowska E (1992). Interneuronal relay in spinal pathways from proprioceptors. *Prog Neurobiol* **38**, 335–378.

Jankowska E, Jukes MGM, Lund S & Lundberg A (1967*a*). The effect of DOPA on the spinal cord. V. Reciprocal organization of pathways transmitting excitatory action to alpha motoneurones of flexors and extensors. *Acta Physiol Scand* **70**, 369–388.

Jankowska E, Jukes MGM, Lund S & Lundberg A (1967*b*). The effect of DOPA on the spinal cord. VI. Half-centre organization of interneurones transmitting effects from the flexor reflex afferents. *Acta Physiol Scand* **70**, 389–402.

Jordan LM (1991). Brainstem and spinal cord mechanisms for the initiation of locomotion. In *Neurobiological Basis of Human Locomotion*, ed. Shimamura M, Grillner S & Edgerton VR, pp. 3–20. Japan Scientific Societies Press, Tokyo.

Kjaerulff O & Kiehn O (2001). 5-HT modulation of multiple inward rectifiers in motoneurons in intact preparations of the neonatal rat spinal cord. *J Neurophysiol* **85**, 580–593.

Koshland G & Smith JL (1989). Mutable and immutable features of paw-shake responses after hindlimb deafferentation in the cat. *J Neurophysiol* **62**, 162–173.

Krawitz S, Fedirchuk B, Dai Y, Jordan LM & McCrea DA (2001). State-dependent hyperpolarization of voltage threshold enhances motoneurone excitability during fictive locomotion in the cat. *J Physiol* **532**, 271–281.

Kriellaars DJ, Brownstone RM, Noga BR & Jordan LM (1994). Mechanical entrainment of fictive locomotion in the decerebrate cat. *J Neurophysiol* **71**, 2074–2086.

Krouchev N, Kalaska JF & Drew T (2006). Sequential activation of muscle synergies during locomotion in the intact cat as revealed by cluster analysis and direct decomposition. *J Neurophysiol* **96**, 1991–2010.

Lafreniere-Roula M & McCrea DA (2005). Deletions of rhythmic motoneuron activity during fictive locomotion and scratch provide clues to the organization of the mammalian central pattern generator. *J Neurophysiol* **94**, 1120–1132.

Lee RH & Heckman CJ (2001). Essential role of a fast persistent inward current in action potential initiation and control of rhythmic firing. *J Neurophysiol* **85**, 472–475.

Lundberg A (1981). Half-centres revisited. In *Regulatory Functions of the CNS. Motion and Organization Principles*, ed. Szentagothai J, Palkovits M & Hamori J, pp. 155–167. Pergamon Akadem Kiado, Budapest.

McCrea DA (2001). Spinal circuitry of sensorimotor control of locomotion. *J Physiol* **533**, 41–50.

McCrea DA, Pratt CA & Jordan LM (1980). Renshaw cell activity and recurrent effects on motoneurons during fictive locomotion. *J Neurophysiol* **44**, 475–488.

McCrimmon DR, Monnier A, Hayashi F & Zuperku EJ (2000). Pattern formation and rhythm generation in the ventral respiratory group. *Clin Exp Pharmacol Physiol* **27**, 126–131.

MacGregor RI (1987). *Neural and Brain Modelling*. Academic Press, New York.

Miller S & Scott PD (1977). The spinal locomotor generator. *Exp Brain Res* **30**, 387–403.

Noga BR, Cowley KC, Huang A, Jordan LM & Schmidt BJ (1993). Effects of inhibitory amino acid antagonists on locomotor rhythm in the decerebrate cat. *Abstr Soc Neurosci* **19**, 540.

Noga BR, Shefchyk SJ & Jordan LM (1987). The role of Renshaw cells in locomotion: antagonism of their excitation from motor axon collaterals with intravenous mecamylamine. *Exp Brain Res* **66**, 99–105.

Orlovsky GN, Deliagina T & Grillner S (1999). *Neuronal Control of Locomotion: from Mollusc to Man*. Oxford University Press, New York.

Perreault MC, Angel MJ, Guertin P & McCrea DA (1995). Effects of stimulation of hindlimb flexor group II afferents during fictive locomotion in the cat. *J Physiol* **487**, 211–220.

Perret C (1983). Centrally generated pattern of motoneuron activity during locomotion in the cat. *Symp Soc Exp Biol* **37**, 405–422.

Perret C & Cabelguen JM (1980). Main characteristics of the hindlimb locomotor cycle in the decorticate cat with special reference to bifunctional muscles. *Brain Res* **187**, 333–352.

Perrier JF, Alaburda A & Hounsgaard J (2003). 5-HT1A receptors increase excitability of spinal motoneurons by inhibiting a TASK-1-like K^+ current in the adult turtle. *J Physiol* **548**, 485–492.

Pratt CA & Jordan LM (1987). Ia inhibitory interneurons and Renshaw cells as contributors to the spinal mechanisms of fictive locomotion. *J Neurophysiol* **57**, 56–71.

Rekling JC & Feldman JL (1998). PreBötzinger complex and pacemaker neurons: hypothesized site and kernel for respiratory rhythm generation. *Annu Rev Physiol* **60**, 385–405.

Rossignol S (1996). Neural control of stereotypic limb movements. In *Handbook of Physiology*, Sect. 12 Exercise: Regulation and Integration of Multiple Systems, ed. Rowell LB & Shepherd J, chap. 12, pp. 173–216. American Physiological Society, Bethesda.

Rybak IA, Lafreniere-Roula M, Shevtsova NA & McCrea DA (2004*a*). A. two layer model of the spinal locomotor CPG: insights from deletions of activity during fictive locomotion. *Abstr Soc Neurosci* 883.3.

Rybak IA & McCrea DA (2005). Computational modeling of the mammalian locomotor CPG. *Abstr Soc Neurosci*, 630.1.

Rybak IA, Paton JFR & Schwaber JS (1997). Modeling neural mechanisms for genesis of respiratory rhythm and pattern. II. Network models of the central respiratory pattern generator. *J Neurophysiol* **77**, 2007–2026.

Rybak IA, Shevtsova NA, Paton JF, Dick TE, St -John WM, Mörschel M & Dutschmann M (2004*b*). Modeling the ponto-medullary respiratory network. *Respir Physiol Neurobiol* **143**, 307–319.

Rybak IA, Shevtsova NA, St-John WM, Paton JFR & Pierrefiche O (2003). Endogenous rhythm generation in the pre-Bötzinger complex and ionic currents: modelling and in vitro studies. *Eur J Neurosci* **18**, 239–257.

Rybak IA, Stecina K, Shevtsova NA & McCrea DA (2006). Modelling spinal circuitry involved in locomotor pattern generation: insights from the effects of afferent stimulation. *J Physiol* **577**, 641–658.

Shefchyk S & Jordan LM (1985). Excitatory and inhibitory post-synaptic potentials in alpha-motoneurons produced during fictive locomotion by stimulation of the mesencephalic locomotor region. *J Neurophysiol* **53**, 1345–1355.

Sirota MG & Shik ML (1973). The cat locomotion elicited through the electrode implanted in the mid-brain. [Article in Russian]. *Fizol Zh SSSR Im I M Sechenova* **59**, 1314–1321.

Smith JC, Butera RJ, Koshiya N, Del Negro C, Wilson CG & Johnson SM (2000). Respiratory rhythm generation in neonatal and adult mammals: the hybrid pacemaker-network model. *Respir Physiol* **122**, 131–147.

Smith JL, Carlson-Kuhta P & Trank TV (1998). Forms of forward quadrupedal locomotion. III. A comparison of posture, hindlimb kinematics, and motor patterns for downslope and level walking. *J Neurophysiol* **79**, 1702–1716.

Stecina K, Quevedo J & McCrea DA (2005). Parallel reflex pathways from flexor muscle afferents evoking resetting and flexion enhancement during fictive locomotion and scratch in the cat. *J Physiol* **569**, 275–290.

Stein PSG (1985). Neural control of vertebrate limb: multipartite pattern generators in the spinal cord. In *Comparative Neurobiology. Modes of Communication in the Nervous System*, ed. Cohen MJ & Strumwasser F, pp. 245–253. John Wiley and Sons, New York.

Stein PSG (2005). Neuronal control of turtle hindlimb motor rhythms. *J Comp Physiol A* **191**, 213–229.

Stein PSG & Grossman ML (1980). Central program for scratch reflex in turtle. *J Comp Physiol A* **140**, 287–294.

Stein PSG & Smith JL (1997). Neural and biomechanical control strategies for different forms of vertebrate hindlimb motor tasks. In *Neurons, Networks, and Motor Behavior*, ed. Stain PSG, Grillner S, Selverston AI & Stuart DG, pp. 61–73. MIT Press, Cambridge, MA.

Streit J, Tscherter A & Darbon P (2005). Rhythm generation in spinal culture. Is it the neuron or the network? *Advances in Network Electrophysiology Using Multi-Electrode Arrays*, ed. Taketani M & Baudry M Springer, New York.

Whelan PJ (2003). Developmental aspects of spinal locomotor function: insights from using the *in vitro* mouse spinal cord preparation. *J Physiol* **553**, 695–706.

Yakovenko S, McCrea DA, Stecina K & Prochazka A (2005). Control of locomotor cycle durations. *J Neurophysiol* **94**, 1057–1065.

Acknowledgements

This study was supported by the Bioengineering Research Partnership grant from the National Institutes of Health (NIH) R01NS048844. I.A.R. and N.A.S. were initially supported by the NIH grants R01NS046062 and R01HL072415. D.A.M. and M.L-R. were also supported by grants from the NIH (R01NS040846) and the Canadian Institutes of Health Research (to D.A.M.) and the Manitoba Health Research Council (studentship to M.L-R.). The authors would like to thank Drs Larry Jordan, Michel Lemay and David Bashor for useful comments and discussion. Ms Maria Setterbom and Ms Sharon McCartney provided technical assistance with figure preparation.